

Imperial College London

Department of Electrical and Electronic Engineering

Final Report 2023

Project Title: **A smart breathing mask for breathing training**

Student: **Matthew Setiawan**

CID: **01917068**

Course: **EIE3**

Project Supervisor: **Prof. Kristel Fobelets**

Contents

1 Abstract	2
2 Acknowledgement.....	3
3 Introduction	4
3.1 Aim.....	4
3.2 Background	4
3.3 Project Objective	4
3.4 Evaluation Plan	5
4 Literature Review.....	6
4.1 Importance of personal devices in monitoring health	6
4.2 Different forms of personal devices to monitor health	7
4.3 Leveraging Personal Devices and Machine Learning for Effective Breathing.....	8
4.4 Techniques for monitoring respiration.....	9
4.5 The use of masks in monitoring breathing	10
4.6 Common Designs for Smart Masks	11
4.7 Conclusion.....	12
5 Analysis and Design of Mask.....	13
5.1 Architecture Overview	13
5.2 Perception.....	13
5.3 Communication	24
5.4 Middleware.....	25
5.5 Application	28
5.6 Conclusion.....	28
6 Analysis and Design of Knitted RIP and RLC Hardware.....	29
6.1 Overview of Knitted Coil and RLC Hardware.....	29
6.2 Initial Observations	31
6.3 Digital Data Extraction into IoT Ecosystem	32
6.4 Conclusion.....	36
7 Visual Demonstration of System.....	37
8 Multi-modal data use cases	39
8.1 Tracking Respiratory Activity with Knitted Coil.....	39
8.2 Observed Correlation with Normal Breathing	44
8.3 Observed Correlation with Fast Breathing.....	47
8.4 Performance of Predictive Models.....	48
8.5 Conclusion.....	52

9	<i>Future Work</i>	53
9.1	Improvements to the Functionality and Form of Mask and Knitted Coil	53
9.2	Improvements to Application Interface.....	54
9.3	Progression in Research and Utilization of Big Data Analytics	55
10	<i>Conclusion</i>	57
10.1	Evaluating Success.....	57
10.2	Summary	58
11	<i>Appendix</i>	59

1 Abstract

Building on Dr Kristel Fobelets' research in knitted breathing coilsⁱ, this project introduces an Internet-of-Things (IoT) based smart breathing mask designed to enhance respiratory health insights by collecting new user data from mask sensors integrated with a respiratory inductance plethysmography (RIP) based knitted coil using a multimodal sensing approach. The current mask features heart rate, acceleration, temperature, and CO₂ sensors positioned around the facial area, enabling monitoring of users' breathing patterns.

The primary objective of this project is to analyse and correlate data from the mask and the knitted breathing coil. By doing so, it will provide a good indication of the effect of respiratory activity on several health parameters, furthermore it will make it possible to predict the inputs from one device using data from the other. For example, if machine learning is employed to detect asthma attacks, the correlated data from just one device could offer enough information to make accurate predictions. This would be useful when wearing both devices is impractical, but data collection remains necessary. Figure 1.1 is the implementation of the smart breathing mask and Figure 1.2 is shows two possible implementations of a knitted coil RIP breathing coil in a garment: One is where the garment is completely knitted as a whole and the other is where the knitted RIP coils are sewn elastically onto a garment.

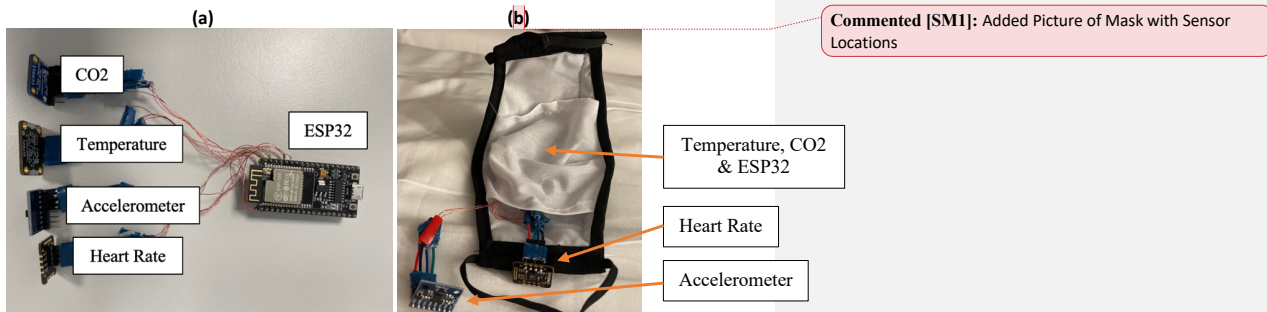


Figure 1.1. (a) Circuitry and labels of commercially available sensors including CO₂, Temperature, Accelerometer and Heart Rate (b) Commercial mask and labels of where main components are positioned



Figure 1.2. Graphical Abstract: Knitted Coil Deviceⁱ

2 Acknowledgement

I would like to express my sincere gratitude to Dr. Kristel Fobelets from the Department of Electrical and Electronics Engineering at Imperial College London for her invaluable guidance and support throughout the course of this project. Her expertise and insights have been instrumental in shaping the direction of this research. I am truly grateful for her mentorship. I would also like to extend my thanks to my friend and colleague in the embedded systems group project, Mr. James Ong. His assistance in designing an initial minimum viable product using a Raspberry Pi. Furthermore, I would like to acknowledge the contributions of Mr. Yinjie, who provided me with the necessary inductor hardware. Our conversations and interactions were incredibly beneficial, as he explained the functionality of the circuit and shared his expertise in this area. His support played a significant role in my understanding of the electrical engineering components of this project. Additionally, I would like to mention Mr. Joshua Lim, with whom I had fruitful communications. He provided me with valuable assistance in explaining various circuit techniques, such as soldering, and explained to me how to use Dr Fobelets' chest phantom device that emulates breathing. His insights and explanations were crucial in expanding my knowledge and enhancing the project's overall quality. I am genuinely grateful to all these individuals for their contributions, guidance, and support. Their expertise and willingness to assist have been instrumental in the successful completion of this project.

Commented [SM2]: Added acknowledgements for Yingjie and Joshua

3 Introduction

3.1 Aim

Commented [SM3]: Added Aims section

The final aim of the project involves completing research and testing on Dr Fobelets' knitted RIP device and identify correlations between the knitted RIP coil to physiological breathing parameters observed by sensors implemented in a face mask.

3.2 Background

The ability to observe respiration is at the core of healthcare diagnosis and monitoring, as numerous health conditions manifest themselves in characteristic breathing patterns. One innovative approach to monitoring respiration, mentioned in the abstract, involves knitted coils that obtain respiration information based on chest diameter changesⁱ. These coils, integrated into wearable garments, detect changes in inductance as a function of circumference, providing valuable insights into breathing patterns with the advantages of being extremely sensitive to minor chest movements.

Smart breathing masks was proposed as an alternative solution to study and read health parameters that knitted coils do not cover, these include CO₂ levels near the mouth, movement, breath temperature, and heart rate. Furthermore, by evaluating the correlation between the read out of the knitted RIP coil and the mask sensors we can enhance information from either implementation through the possible use of predictive models.

Overall, the integration of advanced sensor technology in smart breathing masks in addition to knitted coils not only provides a non-invasive method for monitoring respiration but also has the potential to revolutionize the way healthcare professionals approach respiratory health management. By offering a more in-depth analysis of respiration patterns, smart wearables such as breathing masks and knitted RIP have the potential to significantly improve patient care and outcomes across diverse populations.

The goal of this study is to outline the steps and reasoning behind the creation of the smart breathing mask, and its relationships to knitted coil parameters.

3.3 Project Objective

This project was created with several key objectives that we hope to complete listed below:

1. Create a smart mask sensor system based on multiple commercial sensors considering factors such as effectiveness, reliability, and accuracy.
2. Implement a multimodal sensor system based around the ESP32, ensuring seamless integration of various sensor inputs (including the smart mask sensor system and knitted RIP coil sensor) and efficient data processing capabilities
3. Create an intuitive and user-friendly environment to interact with and display mask sensor and knitted RIP data. The environment should include a web-based interface which supports real-time monitoring, data visualization and data export functionalities.
4. Using the create environment, conduct comprehensive analysis to determine correlations and relationships between the data obtained from the smart breathing mask and knitted RIP.
5. Conduct a thorough evaluation of protentional research directions and applications for the smart mask sensor system and multimodal sensor systems.

3.4 Evaluation Plan

For each of the key objectives listed several evaluation steps will be listed and carried out in detail to determine its success.

Objective 1: Create a smart mask sensor system based on multiple commercial sensors considering factors such as effectiveness, reliability, and accuracy

1. Validate sensor compatibility with the ESP32's I2C communication interface, ensuring their delays and sampling rates are within acceptable ranges.
2. Post-assembly, check for continuous and responsive readings from all sensors. Confirm that readings change appropriately under different test conditions.
3. Upon successful breadboard testing, transition to a compact configuration to fit within the mask chassis. Verify its functionality by conducting the same set of tests.
4. After successful testing of the compact configuration, integrate it into the mask chassis and reaffirm its responsiveness and reliability.

Objective 2: Implement a multimodal sensor system based around the ESP32, ensuring seamless integration of various sensor inputs (including the smart mask sensor system and knitted RIP coil sensor) with a server and efficient data processing capabilities

1. Once the necessary data processing features are developed, cross-verify their measurements with industry-standard devices to ensure consistency and accuracy.
2. Test data transfer from the knitted RIP and mask to the server. Confirm simultaneous measurements are successfully received and processed in the test server.

Objective 3: Create an intuitive and user-friendly environment to interact with and display mask sensor and knitted RIP data. The environment should include a web-based interface which supports real-time monitoring, data visualization and data export functionalities

1. Post data transfer, ensure real-time data from both mask sensor and knitted RIP is appropriately displayed on the web interface.
2. Test data visualization for its accuracy, update speed and ease of interpretation.
3. Evaluate the data export function, ensuring all necessary data can be exported in a user-friendly and accessible format.

Objective 4: Using the created environment, conduct comprehensive analysis to determine correlations and relationships between the data obtained from the smart breathing mask and knitted RIP

1. Utilize the collected data to perform in-depth statistical analyses to identify potential correlations or relationships between smart mask sensor and knitted RIP data.
2. Verify the reliability and accuracy of the analytical tools within the system.

Objective 5: Conduct a thorough evaluation of potential research directions and applications for the smart mask sensor system and multimodal sensor systems.

1. Review relevant literature and studies to explore potential applications and research directions for the smart mask sensor and multimodal sensor systems.
2. Evaluate these potential applications for their feasibility and potential impact, prioritizing based on these evaluations.

Commented [SM4]: Rewritten evaluation plan, more detailed and practical

4 Literature Review

In this chapter, we explore the intersection of personal health technology devices, specifically masks, and their significant contribution to monitoring and improving respiratory health. We begin by discussing the pivotal role of these devices in the health tech landscape in Section 4.1 and 4.2. In Section 4.3, we highlight how technological advancements, including machine learning, are enhancing the capabilities of personal devices. Section 4.4 delves into the various techniques used by both industry and academia for monitoring respiratory health. We then spotlight the unique role of masks in this process in Section 4.5. Finally, in Section 4.6, we focus on the intricate design aspects of these masks.

4.1 Importance of personal devices in monitoring health

Personal devices, such as wearable sensors, are increasingly important in monitoring health and improving overall well-being. These devices offer a range of benefits, including continuous monitoring, early diagnosis, personalised care, and cost-effective treatment, which collectively contribute to better health outcomes for individuals.

Continuous monitoring is a crucial advantage of using wearable sensors ⁱⁱ. These devices can track physiological data throughout the day, such as heart rate, blood pressure, and activity levels. This constant flow of information allows for a more comprehensive understanding of an individual's health, as it captures variations that periodic clinical tests might miss. In addition, with continuous monitoring, it is easier to identify abnormal patterns or deviations from healthy baselines, which can be crucial for early diagnosis and intervention.

Early diagnosis is another benefit offered by personal devices ⁱⁱⁱ. As wearable sensors can detect abnormal conditions in real-time, they enable prompt medical attention, reducing the risk of complications and improving the chances of successful treatment. In addition, early diagnosis often leads to less invasive and more effective treatment options, improving health outcomes and reducing the burden on healthcare systems. For example, a study in the *Guardian* ^{iv} outlined how Fitbit devices could allow doctors to "step in before patients must be sent to the hospital"; beyond offering early diagnosis, this also saves medical costs.

Personalisation is a significant aspect of using wearable sensors for health monitoring ^v. By collecting individualised data, these devices enable healthcare professionals to tailor their approach to each patient, considering their unique circumstances and needs. Personalised care has been shown to lead to better patient engagement, improved compliance with treatment plans, and, ultimately, better health outcomes.

Lastly, wearable sensors can contribute to cost-effective healthcare solutions. By enabling early diagnosis and personalised care, these devices can reduce the overall costs associated with diagnosing and treating illnesses. Additionally, the real-time monitoring offered by personal devices may help prevent unnecessary hospital visits, further lowering healthcare costs.

4.2 Different forms of personal devices to monitor health

The health technology landscape has witnessed a dynamic shift over the past few years, with advancements transcending beyond traditional health monitoring devices to embrace a more personalized and user-friendly approach. A compelling arena where this development is evident is wearable technology, where mainstream devices such as smartwatches, rings, and fitness bands have reshaped how we perceive and interact with health monitoring.

Commented [SM5]: Added section for different devices in monitoring health: watches, rings and clothing

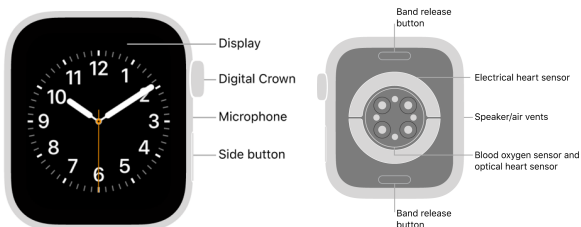


Figure 4.2.1. Apple Watch Diagram ^{vii}

Smartwatches, arguably the most widely recognized health monitoring wearable ^{vii}, have transitioned from being mere extensions of our smartphones to versatile health tools. Brands like Apple (fig. 4.2.1) and Fitbit have revolutionized the market with features including heart rate monitoring, sleep tracking, step counting, and even advanced capabilities such as blood oxygen level monitoring and ECG functions. Accompanying these watches are fitness bands, offering similar functionalities but in a more streamlined and cost-effective form. Prominent players in this field like Garmin and Xiaomi have popularized these devices, effectively democratizing access to health monitoring.

Functionalities	Oura Ring	Motiv Ring
Sleep Duration	Yes	Yes
Sleep Quality Score	Yes	-
Sleep Disturbance Tracking	Yes	Yes
Step Tracking	Yes	Yes
Distance Tracking	Yes	Yes
Heart Rate Sensor	Yes	Yes
Calories Burned	Yes	Yes

Figure 4.2.2. Smart Ring Features (Oura and Motiv) ^{viii}

In contrast to the ubiquity of smartwatches and fitness bands, smart rings represent a less common but equally promising form of wearable technology. Brands like Oura and Motiv have introduced these innovative tools which, despite their compact form, can monitor critical health indicators like heart rate, sleep, and activity levels (fig. 4.2.2). The appeal of these rings lies in their unobtrusiveness, making health monitoring a seamless part of daily life.



Figure 4.2.3. Hexoskin Image and Features

Complementing these commercially available devices are emerging wearable technologies still under research development, like smart clothing. Companies such as Hexoskin (fig. 4.2.3) are pioneering this field with products like smart shirts and bras that monitor heart rate, breathing rate, sleep, and physical activities. This emerging category also includes smart socks that track foot temperature, moisture levels, and gait — a particularly valuable tool for diabetic patients. These cutting-edge devices underscore the convergence of fashion and technology, making health monitoring more personalized than ever before.

4.3 Leveraging Personal Devices and Machine Learning for Effective Breathing Monitoring

Monitoring breathing is essential for maintaining optimal health, as abnormalities in respiration can indicate various illnesses. Respiratory illnesses can range from common conditions ^{ix}, such as asthma and chronic obstructive pulmonary disease (COPD), to more severe disorders, such as lung cancer and pulmonary fibrosis. Early diagnosis of these conditions is crucial for effective treatment and improved health outcomes.

The use of big data analytics and machine learning plays a significant role in enhancing the capabilities of personal devices to detect several of these conditions, removing the need for expensive check-ups. By processing and analysing large volumes of data collected from wearable sensors, advanced algorithms can identify patterns and correlations that might not be apparent through traditional analysis. This can lead to more accurate detection of respiratory abnormalities, enabling timely diagnosis and treatment ^x.

For example, in the case of asthma, a chronic condition characterised by inflammation and narrowing of the airways, monitoring respiratory patterns can help identify early warning signs of asthma exacerbations, allowing for timely intervention and management ^{xi}. Machine learning algorithms can be utilised to analyse the collected data, improving the accuracy and predictive capabilities of the monitoring system.

Similarly, for chronic obstructive pulmonary disease (COPD), early diagnosis and monitoring can lead to better management of symptoms and reduced risk of complications, such as respiratory infections and heart problems ^{xii}. Big data analytics and machine learning can further enhance the effectiveness of wearable sensors in detecting and monitoring COPD by uncovering patterns and trends in respiratory data.

4.4 Techniques for monitoring Respiration

According to the National Health Service (NHS), the “gold standard” technique generally used in healthcare to monitor breathing is called spirometry. Spirometry is a simple test which uses a small machine called a spirometer attached to the mouthpiece. This machine tracks the volume in inhaled and exhaled air^{xiii}. Due to impracticality of spirometry, requiring a mouthpiece to measure air, various other techniques have been developed to measure breathing, including the use of infrared (IR) cameras^{xiv} and inductance plethysmography^{xv}. These methods provide doctors with valuable data to analyse and discover early signs of respiratory problems. By continuously monitoring respiratory patterns, physicians can detect subtle changes in breathing that may indicate the onset of an illness or the worsening of an existing condition.

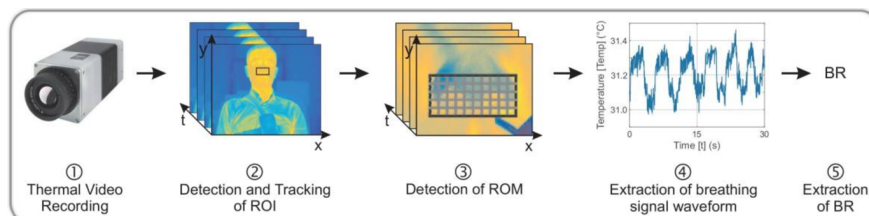


Figure 4.4.1. Utilising Infrared Cameras and Computer Vision to estimate breathing rate (BR): (1) Video Sequence is Recorded (2) Detection of Region of Interest (ROI) is performed (3) Identification of Region of Measurement (ROM) (4) Extract mean temperature of ROM (5) Extract BR from temperature – Figures taken from^{xiv}

Infrared cameras enable doctors to visualise the airflow and temperature changes associated with respiration, which can help identify irregularities in breathing patterns or airflow obstructions. Figure 4.4.1. demonstrates the research and device presented by Dr Pereira from RWTH Aachen University^{xiv} where infrared cameras were used to identify nasal regions, and then using the temperature around the region, extract a temperature time series which could be used to measure breathing rate in a contactless way.

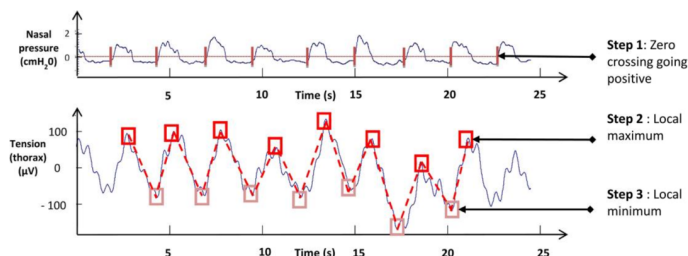


Figure 4.4.2. Nasal Pressure and Respiratory Inductance Plethysmography (RIP) Signals – Figures taken from^{xv}

Another technique called inductance plethysmography^{xv}, offers a quantitative approach to respiratory monitoring, providing information on respiratory rate, volume, and rhythm. Figure 4.4.2. shows the signals that can be obtained using this method, which offers similar information regarding breathing rate to using temperature. Generally using RIP is considered more accurate than infrared (as RIP provides a more direct measurement of breathing rate, focusing on the mechanical aspect of respiration rather than correlations to determine breathing rate) and nearly as accurate as spirometry. It may also be preferable over spirometry as RIP can be integrated into a simple garment which is comfortable

to use over having to wear a mouthpiece. This would be ideal in scenarios where long-term monitoring of breathing may be required.

In both cases, the early detection of abnormalities in respiratory patterns can significantly improve patient outcomes. By identifying potential problems at an early stage, doctors can initiate timely interventions and develop personalised treatment plans, ultimately enhancing the overall quality of care.

4.5 The use of masks in monitoring Breathing

Smart breathing masks have emerged as a potential solution for monitoring respiratory health, offering several advantages over other types of wearable sensors. Face masks provide easy access to critical aspects of respiration, such as respiratory rates and patterns, exhaled breath for measuring volatile biomarkers of disease, respiratory droplets and aerosol particles originating from the wearer or present in the environment, and toxic gases in the environment^{xvi}.

By incorporating sensors into face masks, it becomes possible to continuously analyse respiratory airflows and measure respiratory rates and patterns. This allows healthcare professionals to monitor patients' breathing in real-time, aiding in the early detection of abnormalities and facilitating timely interventions.

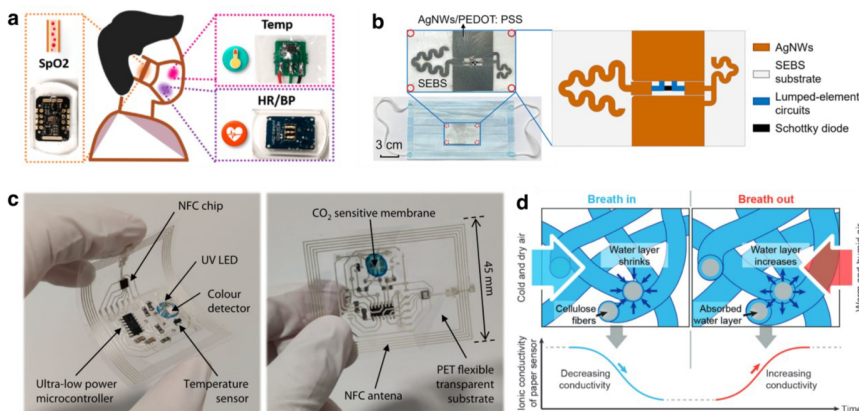


Figure 4.5.1. Passive detection in masks: (a) smart mask integrated with a sensor system to remotely monitor values (b) mask which utilizes deformation to detect coughs (c) mask component with CO₂ sensitive membrane to wirelessly detect CO₂ levels around the facial area with near field communication (NFC) (d) cellulose-based paper mask functioning as a moisture sensor – Figure taken from^{xvi}

Figure 4.5.1. illustrates several techniques for developing sensors and masks that could be useful for the passive monitoring of users^{xvi}. The information these devices provide can be reviewed by healthcare professionals or by automated systems to provide feedback on the user's respiratory functions.



4.7 Conclusion

Overall, this chapter provides a concise exploration of personal devices and methodologies designed to measure respiratory patterns, which is crucial in monitoring pulmonary health. Such knowledge forms the foundation of our project, which is centred on the utilization of smart masks and Respiratory Inductance Plethysmography (RIP) to monitor respiration. Building on this understanding, we will embark on our original research. Our further investigation will seek to unravel the potential synergistic benefits of employing a smart mask in conjunction with a knitted RIP. Further, we aim to examine the correlation between the data obtained through these methods, which could unveil new insights into respiratory health monitoring.

5 Analysis and Design of Mask

This section will primarily discuss the decisions made in designing the smart breathing mask. Section 5.1 will introduce the overall architecture of the device and the following sections will be broken down into the classic IoT layers: Perception, Communication, Middleware and Application. Before the start of this project, a basic version of the device was developed in the ELEC96018 Embedded Systems course, where our team employed a Raspberry Pi integrated with a gyroscope and temperature. In the final year project, I reused some of the frontend software and kept the same gyroscope and temperature sensor but decided to add new sensors and optimize their placing on the body and convert from an inefficient Raspberry Pi to a more suitable ESP32, which will be explained in more detail.

5.1 Architecture Overview

To maintain a structured approach, the analysis and design of the IoT device will be divided into four main categories: perception, communication, middleware, and application layers. The perception layer is responsible for gathering data from the environment and sensors, including power and form factors, as they are closely related. The communication layer, which is sometimes referred to as the network layer, has been renamed to include higher level communication protocols such as HTTP. The communication layer handles the transmission and reception of data, while the middleware layer is responsible for data processing and device management. Finally, the application layer is responsible for providing end-user functionality, including data visualization and analysis. This categorization allows for a clear understanding of the device's architecture and the role of each layer in achieving its intended purpose.

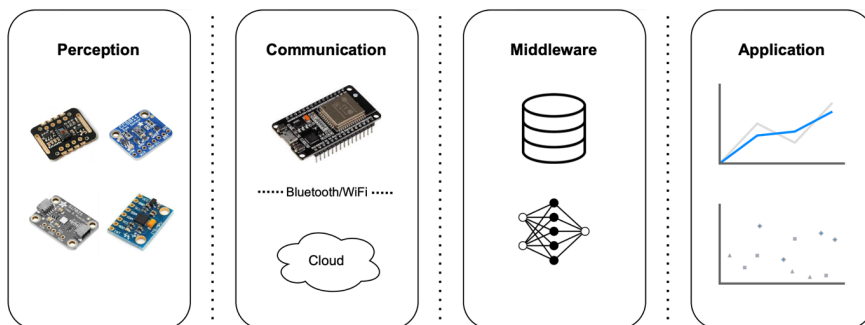


Figure 5.1.1. Visualization of Internet of Things Layers

5.2 Perception

Research was conducted on sensors suitable for a smart breathing mask. The sensors were primarily evaluated based on their accuracy and speed. The sensors were also evaluated based on their suitability for wearable technology, as the sensor package would need to be compact enough to fit into a wearable device for breathing training. The selected sensors are detailed below, along with justifications for their selection based on their specifications, ideal placements, and suitability for the mask.

MAX30102 PPG Sensor ^{xx}



Figure 5.2.1. MAX30102 Pulse and Oximetry Sensor – Figure taken from ^{xx}

Rationale

The MAX30102 is an integrated pulse oximetry and heart rate module. It functions as the primary sensor which will be used to measure heart rate. The core requirements for a heart rate sensor were reasonably accurate measurements, low power requirements and a small form factor.

This sensor was chosen as it fulfilled the core requirements on top of other advantages and features taken from the MAX30102 datasheet:

- Heart rate Monitor and Pulse Oximeter Sensor in LED Reflective Solution
- Tiny 5.6mm x 3.3mm x 1.55mm 14-Pin Optical Module
 - o Integrated Cover Glass for Optimal, Robust Performance
- Ultra-Low Power Operation for Mobile Devices
 - o Programmable Sample Rate and LED Current for Power Savings
 - o Low-Power Heart-Rate Monitor (< 1mW)
 - o Ultra-Low Shutdown Current (0.7 μ A, typ)
- Fast Data Output Capability
 - o High Sample Rates (50-400 samples/second)
- Robust Motion Artifact Resilience
 - o High SNR
- 40°C to +85°C Operating Temperature Range

Data Collection

The MAX30102 PPG sensor outputs a raw signal that needs to be filtered and processed to obtain the heart rate. A PPG sensor uses light to detect blood volume changes in the microvascular bed of tissue. To obtain heart rate from PPG readings, the PPG sensor measures the variations in blood volume and converts them into an electrical signal.

Data Processing

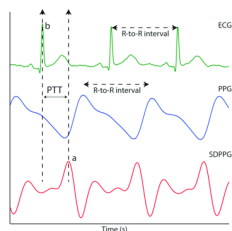


Figure 5.2.2. ECG, PPG and SDPPG Corresponding Signals measured on same test subject – Figure taken from ^{xxi}

Commented [SM6]: Added image and images for all sensors

A simple peak-to-peak slider was initially created to compute heart rate: count the number of peaks in a 5 second window and multiply the value by 12 to obtain final heart rate. However, using the peak-to-

Commented [SM7]: Added ppg/ecg signal comparison

peak method may be prone to noise and is not an industry standard so the Pan-Tompkins algorithm was used instead. The Pan-Tompkins algorithm was originally created for the ECG signal but can be applied with minor changes to make it suitable for PPG signals^{xxii}. The primary adaptation involves modifying the pre-processing step to better accommodate the characteristics of PPG signals. For example, you can use a bandpass filter with appropriate cut-off frequencies (e.g., 0.5 Hz to 4 Hz) to remove noise and baseline wander. Additionally, as PPG signals do not exhibit the same prominent QRS complex as ECG signals shown in Figure 5.2.2, the peak detection method needs to be adjusted to accurately identify systolic (pulse) events in the PPG signal. This can be achieved by using a threshold-based approach or employing more advanced techniques like the continuous wavelet transform or the autocorrelation method. By making these adjustments to the Pan-Tompkins algorithm, it can be effectively applied to PPG signals for estimating heart rate. The following steps provide the steps for a Pan-Tompkins modified heart rate estimator:

1. Pre-processing: Apply a bandpass filter to the raw PPG signal with appropriate cut-off frequencies (e.g., 0.5 Hz to 4 Hz) to remove noise and baseline wander.
2. First derivative: Calculate the first derivative of the filtered PPG signal to emphasize the high-frequency content and rapid changes associated with the pulse events.
3. Square the signal: Square the derivative of the PPG signal to emphasize high-frequency content and accentuate pulse events further.
4. Moving average: Apply a moving average to the squared signal with a window size roughly equivalent to the expected pulse duration. This step integrates the signal, forming an integrated signal emphasizing the pulse events.
5. Peak detection: Identify the peaks in the integrated PPG signal that correspond to the systolic (pulse) events using a threshold-based approach or more advanced methods like the continuous wavelet transform or the autocorrelation method.
6. R-R interval calculation: Measure the time intervals between consecutive peaks in the PPG signal illustrated in Figure 5.2.2. These intervals correspond to the time between successive heartbeats.
7. Heart rate calculation: Calculate the heart rate by taking the average of the R-R intervals and converting it to beats per minute (BPM).

Placement

Due to the nature of the smart breathing mask the sensors need to be placed within the facial area. It is important, however, to ensure that heart rate readings in the facial areas are not significantly worsened.

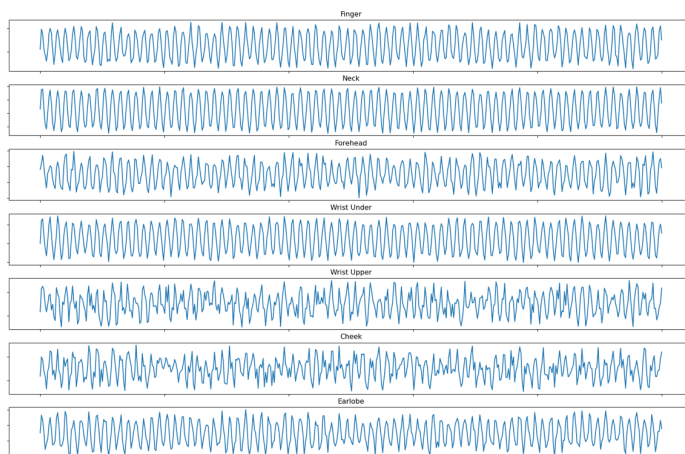


Figure 5.2.3. Raw PPG Signals Measured at Different Areas of the Body of a Volunteer

The signal-to-noise ratio (SNR) is an important factor to consider when placing a PPG sensor. The SNR is the ratio between the power of the desired signal and the power of the background noise. A higher SNR indicates that the desired signal is more distinguishable from the background noise, leading to improved measurement accuracy. Placing the PPG sensor on a body site with a strong response maximizes the signal strength and SNR.

In Figure 5.2.3. the raw PPG measurements from different areas of the body are given. The first 5 readings show common locations where heart rate is measured, and the final two readings show PPG measurements from the cheek and possibly earlobe, which are both within the range of a mask. The values that were obtained were similar to a recent publication by the Faculty of Health Education at the University of Science and Technology at China^{xxiii}.

It is noticeable that in the cheek the signal strength is lower compared to the others indicating an expected lower SNR, however, the SNR is still at a reasonable level whose data would still provide a reliable heart rate reading, given proper pre-processing.

Results

The modified Pan-Tompkins algorithm for PPG signals provides a more reliable and accurate approach for calculating heart rate when compared to the simple peak-to-peak method. While the initial implementation of the peak-to-peak method was easier, the transition to the modified Pan-Tompkins algorithm has led to better results, making it a more suitable choice for PPG-based heart rate detection.

Peak-Peak (bpm)	Pan-Tompkins (bpm)	Apple Watch Validation (bpm)
60	62	65
72	73	69
72	70	74
84	92	89
84	104	101

Figure 5.2.4. Validating Sensor Calculations with Apple Watch

Our readings depicted in Figure 5.2.4 were cross verified with the Apple Watch, whose heart rate detection algorithm is kept private. The peak-to-peak method, which utilized a 5-second window, generated values that were multiples of 12. However, the sliding window approach exhibited some inaccuracies, as a single-beat deviation got magnified by a factor of 12. Conversely, the Pan-Tompkins algorithm yielded results with an error margin of only 4 beats per minute.

CCS811 CO2 Sensor ^{xxiv}



Figure 5.2.5. CCS811 Air Quality and CO2 Sensor – Figure taken from ^{xxiv}

Rationale

The CCS811 sensor is an air quality sensor that can measure volatile organic compounds (VOCs) and equivalent breath CO2 (eCO2) levels. The following are some of the reasons for using this sensor on the device:

1. Monitoring CO2 levels can help assess the quality of the air being inhaled and exhaled during breathing training. High CO2 levels can lead to discomfort and reduced cognitive function while monitoring CO2 levels can help users adjust their breathing patterns for optimal performance.
2. CO2 is a by-product of cellular respiration and tracking its levels can provide valuable feedback on the user's metabolic activity and the efficiency of their breathing technique.
3. Proper CO2 levels are essential for maintaining the body's acid-base balance, which impacts overall health and performance. By monitoring CO2 levels, users can ensure they maintain a healthy balance during their training ^{xxv}.

Data Collection and Processing

The CCS811 sensor outputs digital data in the form of eCO2 and TVOC (total volatile organic compounds) values. These values can be collected and read through an I2C interface, which is compatible with most microcontrollers. For the CCS811, data processing may be required to convert eCO2 levels to the concentration of CO2 in the air (in parts per million) and provide real-time feedback on exhaled air quality and breathing performance. However, this may not be necessary as during monitoring, the relative changes in eCO2 levels can be more important than knowing the precise CO2 concentration. Furthermore, implementing data processing for this sensor could increase complexity and worsen power management for this device.

Placement

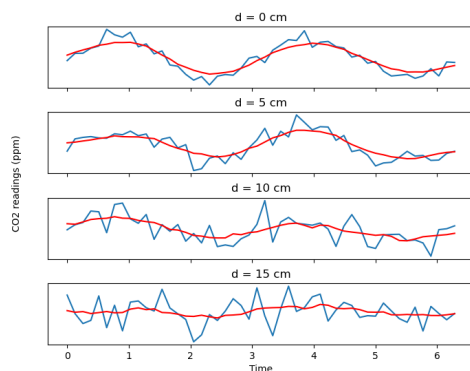


Figure 5.2.6. CO2 readings with varying distances (d) to mouth: Raw Values (blue) and Filtered Values (red)

Commented [SM8]: Added CO2 readings and varied distance from mouth

The ideal placement for the CCS811 sensor in a smart breathing mask would be in the front of the mouth. Figure 5.2.6 shows results when varying the distance of this sensor from the mouth: by 15cm the CO₂ values are almost completely engulfed by noise. The reason for this is because, although the white noise remains roughly the same, the impact of our breath significantly decreases resulting in a decreasing SNR.

Si7021 Humidity and Temperature Sensor ^{xxvi}



Figure 5.2.7. Si7021 Humidity and Temperature Sensor – Figure taken from ^{xxvi}

Rationale

The Si7021 is a digital humidity and temperature sensor that provides accurate and reliable readings. A few of the reasons for tracking temperature include:

1. Monitoring temperature is very common when dealing with patients with breathing problems including asthma ^{xxvii}. It is also indirectly linked to other conditions such as diabetes which may affect blood flow and indirectly impact breath temperatures ^{xxviii}.
2. Temperature regulation is essential for optimal performance during training. By tracking temperature, users can ensure they maintain a comfortable environment for their breathing exercises.
3. The temperature of inhaled air is usually lower than exhaled air because inhaled air is at the ambient temperature, while exhaled air has been warmed by the body. This allows us to use temperature to get insights on breaths.

The Si7021 tracks respiration very similarly to the infrared camera temperature method described in section 4.3. A disadvantage of this method is that it only provides a single temperature value unlike the camera which provides the temperatures of the breath at different areas of the lung. However, this method is much simpler and cost effective to implement in a mask unlike an infrared camera.

Data Collection and Processing

The Si7021 sensor outputs digital data in the form of temperature and humidity values. The data can be collected and read through an I₂C interface, compatible with the ESP32. Minimal data processing is needed since the sensor provides temperature readings in Celsius, and we are mainly interested in relative temperatures.

Placement

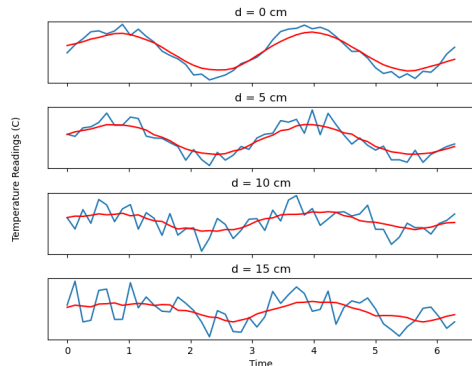


Figure 5.2.8. Temperature readings with varying distances (d) to mouth: Raw Values (blue) and Filtered Values (red)

Commented [SM9]: Added temperature readings and varied distance from mouth

Since we are more interested in monitoring the temperature of the inhaled and exhaled air, placing the sensor near the mouth within the mask would be most appropriate. In Figure 5.2.8 the same experiment with the CO₂ sensors were carried out and similar results were obtained, although we could observe a slightly stronger SNR in temperature compared to CO₂ at all distances.

MPU6050 Accelerometer and Gyroscope ^{xxix}



Figure 5.2.9. MPU6050 Accelerometer and Gyroscope Sensor – Figure taken from ^{xxix}

Rationale

Incorporating the MPU6050 can provide insights about breathing by detecting subtle movements and vibrations associated with respiration. The MPU6050 is a popular and cost-effective inertial measurement unit (IMU) that combines a 3-axis gyroscope and a 3-axis accelerometer, enabling it to measure both linear acceleration and angular velocity. By placing the sensor on the chest, abdomen, or other relevant body parts, it can monitor the expansion and contraction of the respiratory muscles, thus providing valuable information about breathing patterns, rate, and depth. This approach has been employed in various research studies to develop non-invasive and wearable respiratory monitoring systems ^{xxx}. Using the MPU6050 for breath monitoring can potentially help in assessing respiratory health, tracking physical activity, and monitoring sleep quality, among other applications.

Another use for the MPU6050 would be in motion artifact correction when tracking breathing with sensors. It works by capturing data related to body movements that may cause distortions in the respiratory signal. By measuring acceleration forces, it can detect both the intensity and direction of motion. This motion data can then be used to filter out or correct any artifacts in the respiratory signal, enhancing the accuracy of breath tracking and ensuring the signal reflects true physiological breathing patterns rather than movements or other non-breathing related factors ^{xxxi}.

Data Collection and Processing

The MPU6050 outputs digital data, in the form of 16-bit signed integers (2's complement representation), for each of the axes. These values represent the measured angular velocities (for gyroscope) and linear accelerations (for accelerometer) along the X, Y, and Z axes. The data can be collected and read through an I2C interface, compatible with the chosen microprocessor. Very minimal data processing is needed for this sensor, although it is quite common to take the L2 norm shown in equation 5.2.10 of the three axes to simplify analysis further^{xxxii}.

$$N = \sqrt{x^2 + y^2 + z^2} \quad (5.2.10)$$

Where:

- N is the L2 norm
- x is the acceleration on the x-axis
- y is the acceleration on the y-axis
- z is the acceleration on the z-axis

Placement

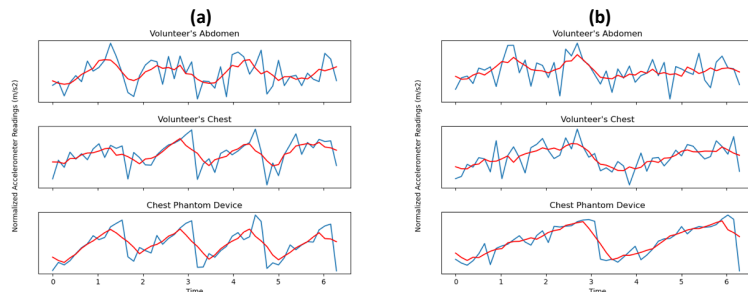


Figure 5.2.11. MPU6050 readings on different areas of a healthy volunteer and on a chest phantom device: Fast Breathing (a) and Normal Breathing (b)

The MPU6050 inertial sensors, which include accelerometers and gyroscopes, can be positioned on various parts of the body to capture breathing information. However, breathing would typically correlate with movements in areas close to the chest and abdomen^{xxx}. Therefore, instead of placing the MPU6050 on facial areas, it would be more logical to attach them to a t-shirt containing the knitted RIP. Figure 5.2.11. presents some readings from the MPU6050 placed on different areas of a healthy volunteer and when attached to a chest phantom device. Observing the differences between the readings on a chest phantom and a human volunteer, we can deduce that not only does the signal-to-noise ratio (SNR) change, but the nature of the noise also varies. A human volunteer may be more prone to movement, which can affect the accelerometer readings, whereas this type of noise is not present with a chest phantom device. Furthermore, we also notice a higher SNR during rapid breathing. This could be because the MPU6050 measures acceleration, which would naturally be greater during faster breathing.

Commented [SM10]: Added MPU readings on different areas of body and when taped into the chest phantom

ESP32 Microcontroller

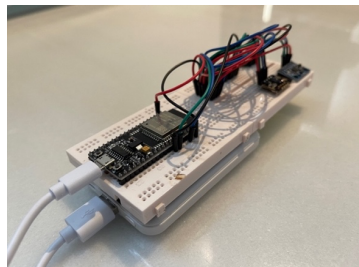


Figure 5.2.12. Initial integrated prototype: ESP32 and sensors on breadboard, powered by micro-USB to power bank

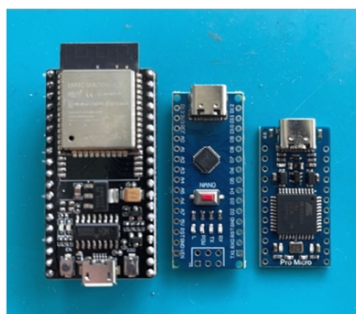


Figure 5.2.13. Development Boards under Consideration (Left to Right): ESP32, Arduino Nano, Pro Micro

Whilst the IoT system developed in the ELEC96018 Embedded Systems course used a Raspberry Pi due to functional requirements, the ESP32 development board (as shown in Figure 5.2.13) was selected for its versatility and compatibility with a wide range of sensors and peripherals, and for its built-in Wi-Fi and Bluetooth capabilities, which allowed for easy communication with a server. Although the Raspberry Pi Zero was originally considered due to its ease of use, it had several severe limitations. Compared to the ESP32, the Pi Zero had higher power consumption, a larger form factor, limited real-time performance, and required additional modules to add Wi-Fi and Bluetooth capabilities. Overall, the ESP32 proved to be the better choice for integrating the sensors and establishing communication with the server; Its selection helped to ensure the project's success.

	ESP32	Arduino Nano	Pro Micro
Wi-Fi Capability	Included	Not Included	Not Included
Bluetooth	Included	Not Included	Not Included
Size	Large	Medium	Small
Clock Speed (MHz)	240	16	16
GPIO Requirements	Fulfilled	Fulfilled	Fulfilled
Flash Memory	Fulfilled	Fulfilled	Fulfilled

Table 5.2.14. Comparison of Development Boards

After considering several development boards from the Arduino family, we analysed their specifications in Table 5.2.14. All the boards met the GPIO and Flash Memory requirements, but our final decision was based on speed, communications capabilities, and size.

The Arduino Nano was eliminated from consideration because it didn't offer a speed advantage over the Pro Micro or ESP32, and it was also larger than the Pro Micro. We then compared the Pro Micro and ESP32. Initially, we considered attaching a network interface card (NIC) to enable Wi-Fi on the Pro Micro. However, this would have resulted in two devices, which would not significantly decrease the size and could potentially increase the error rate. Therefore, we decided that the ESP32 was the best option. In summary, we selected the ESP32 board as it met the requirements for GPIO, Flash Memory, and provided the desired speed, communication capabilities (built-in Wi-Fi and Bluetooth), and a suitable size for our project.

Form Factor

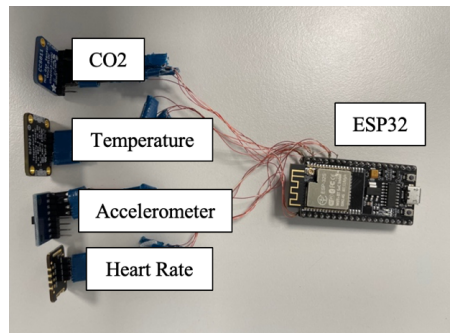


Figure 5.2.15. Compact Setup of Prototype

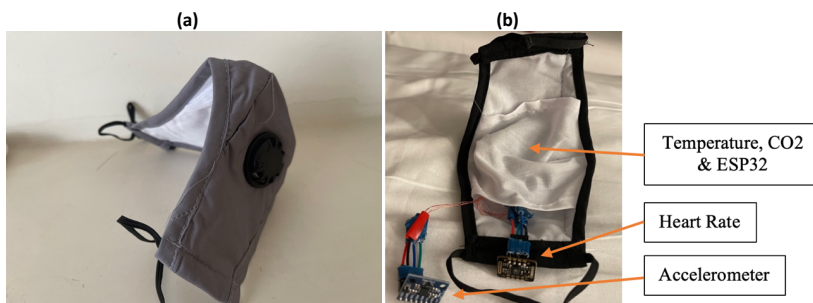


Figure 5.2.16. Chassis of Prototype: (a) Outside of Mask (b) Inside of Mask with labelled components

After creating and testing the initial system depicted in Figure 5.2.12, the unnecessary components, such as thick wiring and breadboard, were removed and replaced with thinner wiring directly soldered to the ESP32, as shown in Figure 5.2.15. With this setup, it would be possible to enclose it in a compact mask chassis illustrated in Figure 5.2.16.

5.3 Communication

The ESP32 is built with support for both Bluetooth 5.0 and 802.11 b/g/n Wi-Fi protocols allowing it to transmit data over short and long distances.

Bluetooth

When it comes to Bluetooth, the ESP32 supports the latest version of Bluetooth, Bluetooth 5.0. This allows it to establish a wireless connection with other Bluetooth-enabled devices such as smartphones, laptops, and IoT devices. The ESP32 also supports Bluetooth Low Energy (BLE), which is a power-efficient protocol that allows for long battery life in devices that use it.

Wi-Fi

When it comes to Wi-Fi, the ESP32 supports 802.11 b/g/n Wi-Fi protocols, which means it can connect to almost any Wi-Fi network. This allows it to send and receive data wirelessly over the internet or local network. Differently from Bluetooth, a communication protocol needs to be used to establish communication between the ESP32 and the web server. The three most common communication protocols which come to mind are HTTP, MQTT and COAP. As testing the speed of these three protocols could be done quite easily, testing was done during this initial analysis and design phase rather than further down the line where code could be larger and more complex. The results of sending strings of different byte sizes are summarized in figure 5.3.1:

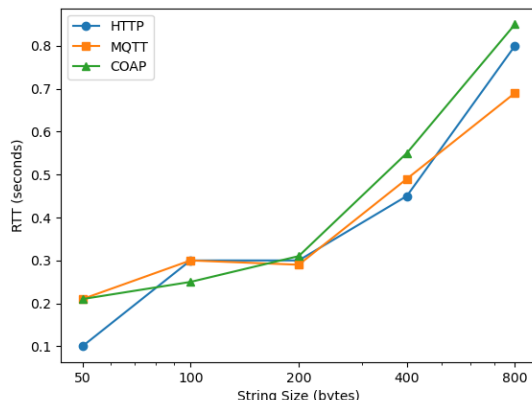


Figure 5.3.1. RTT vs Payload of Different Communication Protocols

Figure 5.3.1 shows that HTTP is the optimal choice for the thesis project. The analysis of the payload vs. round trip time (RTT) suggests that HTTP is the fastest and most suitable protocol for the application, which requires sending small payloads. In addition, HTTP GET requests are simple to implement and scalable, making them an ideal choice for the project's communication requirements. The well-established nature of HTTP as a protocol for the web makes it a familiar and straightforward option to use, with simple implementation and easy integration with web servers and APIs. Overall, the use of HTTP will allow the project to meet its communication needs efficiently and effectively.

5.4 Middleware

In the development of this mask, a significant component to highlight is the implementation of the middleware layer. This layer serves as the bridge between raw sensor data and the extraction of meaningful health indicators, paving the way for enhanced functionality of the mask. The middleware layer's fundamental role is to enable real-time monitoring and analysis of vital signs. It works by interpreting raw sensor data and converting it into practical and understandable information such as heart rate, a process detailed in the previous section. Moreover, this layer also involves the management and transfer of data.

Data Processing

Filtering

The two common filtering techniques used in finance ^{xxxiii} are exponential in eq. (5.4.1) and Gaussian filtering in eq. (5.4.2):

$$K(\sigma, x) = \frac{1}{\sqrt{2\pi}\sigma} e^{-\frac{x^2}{2\sigma^2}} \quad (5.4.1)$$

$$y[n] = \alpha x[n] + (1 - \alpha)y[n - 1] \quad (5.4.2)$$



Figure 5.4.3. Yahoo Finance FTSE ^{xxxiii}: Real Price (Blue), Gaussian Kernel (Red), Exponential Kernel (Purple)

Although both kernels are effective at reducing noise and improving the quality of the data, they offer slightly different results. Gaussian kernels are not centred around the most recent data and are more responsive to small variations in the data. On the other hand, exponential kernels place most weight on most recent information and are more responsive to larger trends in the data. This can be further observed when carefully looking at Figure 5.4.3. This shows that exponential filtering tends to provide a smoother result with a slight forward shift in the data, while Gaussian filtering tends to preserve more of the original signal's features and is centred around past information. Given that we aim for the data to be as recent as possible, an exponential filter may be preferable.

Breathing Rate

The CCS811 CO2 Sensor, Si7021 Temperature Sensor, and MPU6050 gyroscope as demonstrated above were able to be used to track breathing. The following data in Figure 5.4.4 show corresponding temperature and CO2 levels were collected and overlapped with exhale periods.

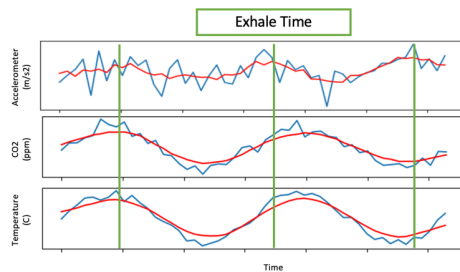


Figure 5.4.4. Simultaneous Accelerometer, CO2, Temperature Readings overlapped with Exhales

Commented [SM11]: Added MPU results

We observed that the accelerometer responds quicker to exhalation times, as it is directly correlated with chest movements. Meanwhile, CO2 and temperature sensors appeared to respond more slowly, which is understandable considering these sensors may require time to warm up and adjust to the changes.

A straightforward method to track breathing could be the implementation of a sliding peak counter. This approach would involve counting local maxima within a 5-second timeframe, then multiplying the result by 12 to derive the breathing rate in breaths per minute.

Data Management

Minimal data had to be kept for our system: device data and user data. The following Figure 5.4.5. highlights the entity relationships between elements in the database.

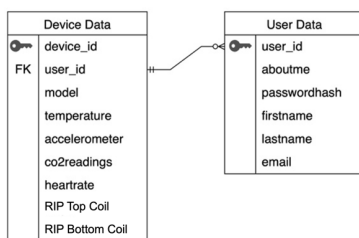


Figure 5.4.5. Database Entity Relation

In managing data, it was important to create a system that was scalable and easily modifiable. Each device would be assigned a unique ID, like a MAC address, users can then create their account and link their designated account to the specified device ID. This creates a system where multiple users can connect to multiple different devices as well instead of creating a system that only works for one individual.

Data Security

There were several measures that needed to be taken to reduce the number of vulnerabilities in such IoT devices, these included packet sniffing, password attacks, SQL/XSS injections or firmware vulnerabilities. The following measures were taken to reduce the likelihood of these occurring.

During transmission, we decided to use public key cryptography techniques ^{xxxiv}, where our web server would launch a publicly accessible API to obtain the public key and the private key would be generated purely on the server side. Hence the following steps were taken for the transmission of data:

1. ESP32 obtains RSA public key and encrypts the data before transmission
2. Data is sent over HTTPS using GET requests
3. The server contains a private key used to decrypt the transmitted data

To secure the passwords in my database, I used a technique called password hashing with salt ^{xxxv}. First, I generated a unique random salt for each user's password. Then, I concatenated the salt with the password and passed it through a cryptographic hashing function. The resulting hash was then stored in the database. By using a unique salt for each user, I ensured that even if two users had the same password, their hashes would be different, which makes it more difficult for attackers to reverse-engineer the passwords. Additionally, by using a strong cryptographic hashing function, I ensured that it would be computationally difficult and time-consuming for attackers to guess the original password from the hash. This approach provided an additional layer of security to my password database and helped protect my users' passwords from being compromised.

To prevent SQL injections, it is important to maintain the use of prepared statements throughout my site. Furthermore, SQLMap can be run against the web server to ensure that no SQL vulnerabilities were found.

Given that the site is developed using the Django framework, cross-site scripting attacks are usually protected against, however, it is always important to maintain the latest firmware to prevent bugs in these frameworks.

5.5 Application

Data Visualization

To display real-time data on the website, Chart JS and AJAX can be used in the application layer of the system. The following steps show how data goes from the sensors all the way to the frontend system:

1. The ESP32 reads sensor data.
2. The data, including the device ID, is sent to the backend via HTTPS for storage in the database.
3. When a user requests real-time data, the front end sends an AJAX request to the backend.
4. The backend responds to the AJAX request with the latest sensor data from the database.
5. The frontend JavaScript updates the UI with the received sensor data and renders it in charts using Chart JS.

Interaction

In the application layer of the smart breathing mask, the user experience is designed as follows:

1. Account creation: The user begins by downloading the companion app for the smart breathing mask and creating an account. This involves entering personal information such as name, age, weight, and height, which will be used to tailor insights and recommendations.
2. Device pairing: Next, the user pairs their smart breathing mask and knitted coil with the application. This is typically done through a Bluetooth or Wi-Fi connection. Once connected, the app will display the status of both devices and sync data in real time.
3. Calibration: The calibration process is initiated through the app, guiding the user through a series of steps to ensure accurate measurements between the smart breathing mask and the knitted coil. This may include performing specific activities or breathing exercises to generate a baseline of data for comparison.
4. Viewing key values and insights: Once calibration is complete, the user can access a dashboard within the app that displays real-time data on breathing rate, heart rate, CO₂ levels, movement, and temperature. The dashboard also provides insights and recommendations based on the data, helping the user understand their respiratory health and make informed decisions about their training and overall well-being.
5. Saving calibration data: After the initial calibration, the app stores the calibration data for future use. This allows users to switch between using the smart breathing mask and the knitted coil for single predictive use. By leveraging the stored calibration data, the system can predict all values using only one of the devices, providing a flexible and convenient monitoring solution.
6. Ongoing interaction: Users can continue to interact with the app, updating their personal information, recalibrating devices as needed, and reviewing the insights generated by the smart breathing mask and knitted coil. The app may also include features such as goal setting, progress tracking, and sharing capabilities, further enhancing user engagement, and promoting a healthy lifestyle.

5.6 Conclusion

Overall, the smart mask was designed successfully, with all sensors seamlessly integrating and delivering rapid readings. The system's data processing capabilities proved efficient, effectively handling crucial functions such as heart rate monitoring and air filtration. The design of the frontend application was also executed successfully, enabling the real-time visualization of data.

6 Analysis and Design of Knitted RIP and RLC Hardware

The following section will provide a detailed introduction to the Knitted Coil device created by Dr. Fobeletsⁱ and techniques used to integrate this device into our existing IoT system. It will also give an overview of the methods used to extract useful insights from this device, followed by a validation of the expected and actual measurements.

6.1 Overview of Knitted Coil and RLC Hardware

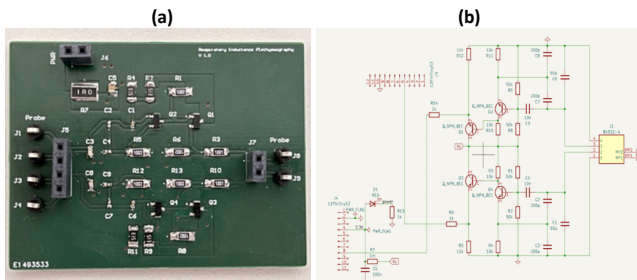


Figure 6.1.1. (a) PCB of two Colpitts Oscillators (b) Schematic of two Colpitts Oscillators



Figure 6.1.2. Shirt Knitted with Inductor Coils to be connected to Colpitts Oscillators

A Colpitts oscillator (fig 6.1.1) designed by Mr Yingjie, is an electronic oscillator that utilizes a combination of inductors (L) and capacitors (C) to create an oscillating radio frequency (RF) signal^{xxxvi}. The fundamental operational principle relies on positive feedback. A phase shift of 180 degrees is initiated by the LC network (a combination of inductors and capacitors), with the transistor or amplifier contributing another 180 degrees. This results in a total phase shift of 360 or 0 degrees, essential for continuous oscillations.

The oscillation frequency is dependent on the inductor and capacitors' values. This resonant frequency is calculated by the following (eq. 6.1.3) for a parallel LC circuit.

$$f = \frac{1}{2\pi\sqrt{LC}} \quad (6.1.3)$$

Here, L signifies inductance and C signifies capacitance. The frequency is inversely proportional to the inductance's square root, indicating that an increase in inductance will reduce the frequency and vice versa.

The inductors of the Colpitts oscillator are knitted and integrated into a shirt (fig. 6.1.2) worn by a person and will expand and contract in sync with the individual's breathing, causing a change in the inductor's diameter and consequently, its inductance (eq. 6.1.4). This change in inductance modifies the oscillator's frequency, enabling the tracking of the individual's breathing rate and pattern by measuring these frequency changes.

The mathematical relationship illustrating this principle shows that inductance is proportional to the diameter's square:

$$L = \frac{N^2 \mu A}{I} \quad (6.1.4)$$

The diagram shows a coil with three turns labeled N=1, 2, 3, ... A horizontal double-headed arrow above the coil indicates its length L . To the right of the coil, a vertical double-headed arrow indicates its area A . A red bracket on the right side of the coil encloses the formula $D = 2\sqrt{\frac{A}{\pi}}$, where D represents the diameter.

where:

- L is the inductance
- μ is the permeability of the core material
- N is the number of turns in the coil
- A is the area of coil
- I is the length of the coil.

The self-inductance of the coil follows a similar relationship to eq. 6.1.4^{xxxvii}. When the wearer breathes in, the coil expands, increasing its diameter, area and inductance and therefore decrease the resonant frequency (according to eq. 6.1.3). The opposite happens when the wearer breathes out.

According to the given reasoning, we expect similar results when observing the voltage outputs of the connected PCB in Figure 6.1.1.

Commented [SM12]: Added illustration for coil

6.2 Initial Observations

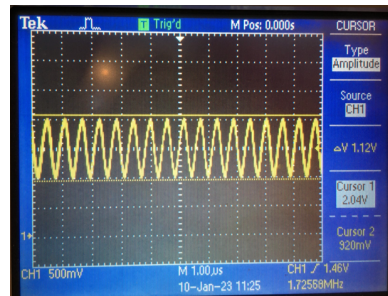


Figure 6.2.1. Applying Fast Fourier Transform (FFT) using Oscilloscope to Output Signals

Initial observations of the Fast Fourier Transform (FFT) (fig. 6.2.1) confirmed the original hypothesis: breathing in reduces peak frequency and vice versa. The table below gives more detailed insights into the changes in peak frequency depending on inhalation or exhalation:

Reading No.	Peak Frequencies (MHz)			
	Exhale Top Coil	Inhale Top Coil	Exhale Bottom Coil	Inhale Bottom Coil
1	1.381	1.360	1.355	1.350
2	1.385	1.362	1.357	1.349
3	1.381	1.359	1.358	1.351
4	1.384	1.364	1.353	1.348
5	1.380	1.365	1.354	1.348
Average	1.382	1.362	1.355	1.350

Table 6.2.2. Peak Frequencies during Exhales and Inhales

As observed in Table 6.2.2 the peak frequencies during inhales and exhales have very clear changes in line with the initial hypothesis. It was also noticed that the top coil had a stronger response, this response may be due to a variety of factors such as size of user's chest and abdomen and whether the user is a chest or abdomen breather.

6.3 Digital Data Extraction into IoT Ecosystem

Following the observation of some relationships from the device, this section focuses on how to digitally extract the data for comparative analysis into our server and originally created ecosystem shown in the previous sections. During this process, three methods were attempted and two of them worked favourably well.

ESP32 Voltage Read In

The initial approach involved using the GPIO (General-Purpose Input/Output) pins of an ESP32 microcontroller to read voltage levels to evaluate the signal produced by the Colpitts oscillator. By connecting the GPIO to the oscillator, the intention was to interpret the signal by sampling the voltage levels and feeding this data into a Fast Fourier Transform (FFT) algorithm.

The FFT is an algorithm that computes the discrete Fourier Transform (DFT) of a sequence, or its inverse ^{xxxviii}. The DFT is defined as:

$$X[k] = \sum_{n=0}^{N-1} x[n] e^{-j2\pi kn/N} \quad (6.3.1)$$

Where:

- $X[k]$ are the frequency bins of the FFT.
- $x[n]$ is the time-domain input signal.
- e is the base of the natural logarithm.
- j is the imaginary unit.
- N is the number of points in the FFT.
- k and n are the frequency and time indices, respectively.

Once the FFT was applied, the next step was to determine the peak frequency in the resulting spectrum, which would correspond to the resonant frequency of the oscillator. This resonant frequency would then give us the breathing rate of the person wearing the shirt with the knitted inductor.

However, this approach encountered a significant challenge due to the ESP32's limitation in reading MHz level frequencies. The ESP32, while powerful for a microcontroller, cannot accurately sample at the speeds required to read MHz frequencies directly due to its hardware constraints and the Nyquist-Shannon sampling theorem, which states that to properly sample a signal, the sampling frequency must be at least twice the highest frequency component of the signal.

Digital PicoScope Read In

A simple solution but not very wearable solution would be to use a digital PicoScope or simply stronger hardware that could read voltages at MHz speeds. The digital PicoScope 2000 which was being used, offered an API that would stream data at 31 million samples per second^{xxxix}. Since this is way above the theoretical requirement of around 2.76 million samples per second (based on Nyquist's theorem and our observed peak frequency in section 6.2), the PicoScope is expected to provide decent readings.

The FTT readings with the PicoScope are shown in Figure 6.3.2. The frequencies plotted are those with the greatest FTT magnitude. These validation measurements were quite accurate to our original measurements in 6.2.2 and showed clear variations between inhalation and exhalation.

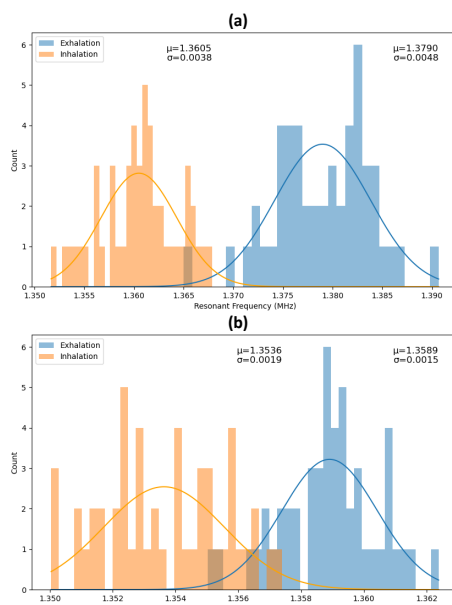


Figure 6.3.2. Validation Measurements of Frequencies during Exhales and Inhales for PicoScope on human volunteer: (a) Top Coil (b) Bottom Coil

The plots in Figure 6.3.2 were obtained from a healthy volunteer breathing normally. The standard variation is a result of both the volunteers' normal breathing variability as well as the variability of the read-out system. To improve measurements, we can use a chest phantom shown below (fig. 6.3.3).

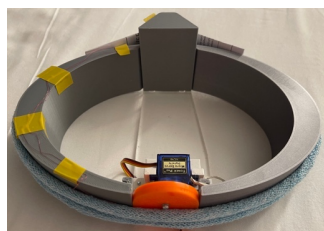


Figure 6.3.3. The chest phantom holding a test coil. The oval disk is connected to a small motor to rotate it around its axis over programmed angles and with a given speed.ⁱ

Commented [SM13]: Added chest phantom image

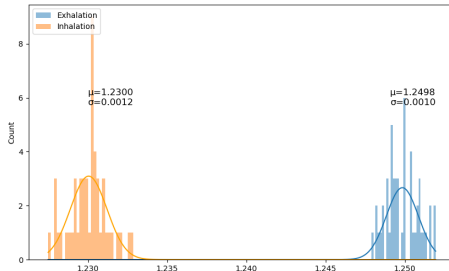


Figure 6.3.4. Validation Measurements of Frequencies during Exhalations and Inhalations for PicoScope on chest phantom

The main difference observed in the chest phantom (fig. 6.3.4) was the much lower variance, this is expected as a machine would produce much more accurate results.

Commented [SM14]: Added validation measurements with chest phantom

ESP32 Pulse Counter (PCNT) Module

Despite performing very well and potentially having better performance than ESP32s, the Digital PicoScope solution was not ideal because of cost and portability issues. A solution that was not considered utilizing the built in PCNT module of the ESP32¹¹. This module allows for the generation of a signal with a specific duty cycle that can be utilized in controlling a wide variety of devices. The following shows the general algorithm and steps used to utilize the PCNT module for frequency.

- 1: Configuration:**
Initialize the PCNT module by configuring the input pin, counter mode, and other parameters.
Select the PCNT unit (there are multiple units available in ESP32) and assign a specific input signal to it.
- 2: Counter mode selection:**
Choose the counter mode based on your requirements. PCNT can be configured in different modes such as single pulse, dual pulse, or quadrature encoder.
- 3: Event detection and counting:**
Enable the PCNT module and start the counter.
Configure the PCNT module to count rising or falling edges (or both) by setting appropriate filters and thresholds.
As the input signal arrives, the PCNT module detects the rising and/or falling edges and increments the corresponding counter(s).
- 4: Interrupt generation:**
Configure the PCNT module to generate interrupts based on specific conditions.
For example, you can set an interrupt to trigger when a certain number of edges are counted or when the counter reaches a predefined value.
- 5: Frequency calculation:**
To compute the frequency of the incoming signal, you can use the counts accumulated by the PCNT module over a specific period.
Determine the elapsed time since the last frequency calculation (using a timer, for example).
Divide the number of counted edges by the elapsed time to obtain the frequency.

Algorithm 6.3.5. Algorithm to Obtain Frequency using PCNT module

Using Algorithm 6.3.5 the frequency could be measured moderately well, however in the process of frequency reading, issue was encountered with spiking frequencies. To this issue, I chose to implement

a median filter (eq. 6.3.6). A median filter works by storing several of the most recent readings and then selecting the median value from this list. This way, it effectively eliminated any sudden spikes in the frequency, providing a much more stable and accurate reading. This was particularly effective as the median filter doesn't require many computational resources and is straightforward to implement.

$$f'[t] = \text{median}(f[t-k], \dots, f[t-2], f[t-1], f[t]) \quad (6.3.6)$$

Where:

- $f'[t]$ is the filtered frequency at time t
- $f[t]$ is the raw frequency at time t
- k is the window size

The following figure 6.3.7 gives the validation measurements when using the PCNT module on a healthy volunteer breathing normally.

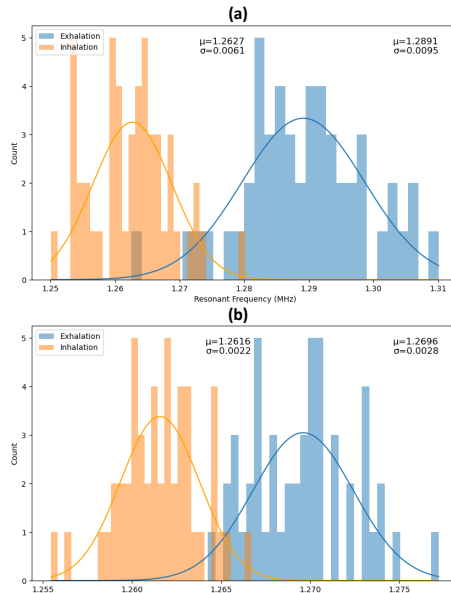


Figure 6.3.7. Validation Measurements of Frequencies during Exhales and Inhales for PCNT Module on Volunteer: (a) Top Coil (b) Bottom Coil

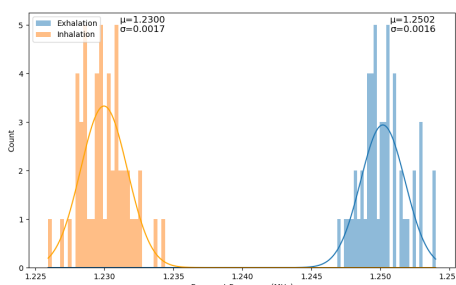


Figure 6.3.8. Validation Measurements of Frequencies during Exhales and Inhales for PCNT Module on Chest Phantom

Commented [SM15]: Added validation measurements with chest phantom

Evaluating the standard deviation when comparing the PCNT Module and PicoScope indicated that there was a small reduction in performance: the variance for the PCNT data for both human volunteers and chest phantom shown in figures 6.3.7 and 6.3.8 was slightly higher across the board indicating a lower SNR. Nonetheless the performance still shows a strong difference in resonant frequencies between inhalation and exhalation, and the overall benefits of using an ESP32 in cost and portability makes it a more feasible choice of hardware.

6.4 Conclusion

Overall, the execution of our data collection strategy was remarkably efficient. To start with, we successfully leveraged the ESP32 PCNT module to extract the general frequency of the knitted coil. Subsequently, the resulting frequencies demonstrated expected behaviour consistent with inductors and RLC circuits, and we effectively applied filters to further diminish spectral noise. Lastly, the data was seamlessly integrated with our pre-existing IoT system, enabling the simultaneous and effortless collection of data from both the mask and the knitted coil.

7 Visual Demonstration of System

Commented [SM16]: New section just on the software

The following section will provide a few illustrations of the product's software in practice.

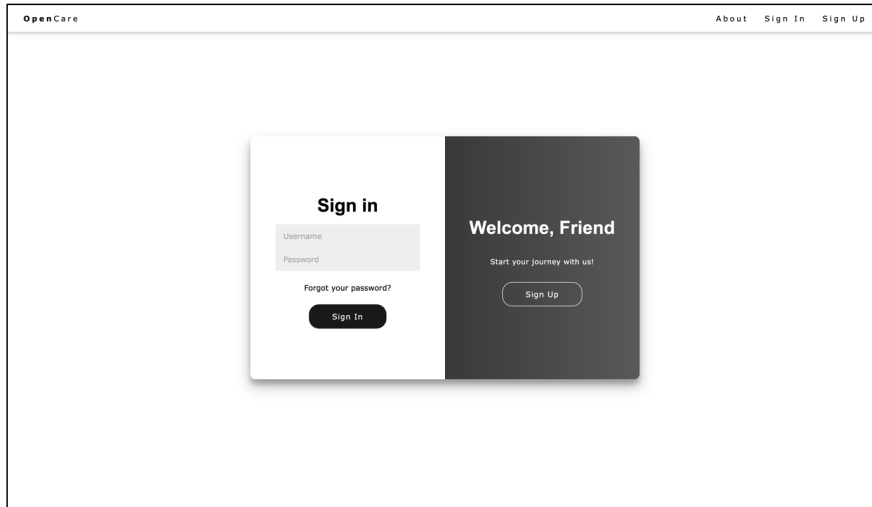


Figure 7.1. Login Screen



Figure 7.2. Linking Device Page



Figure 7.3. Accessing Live Data Page

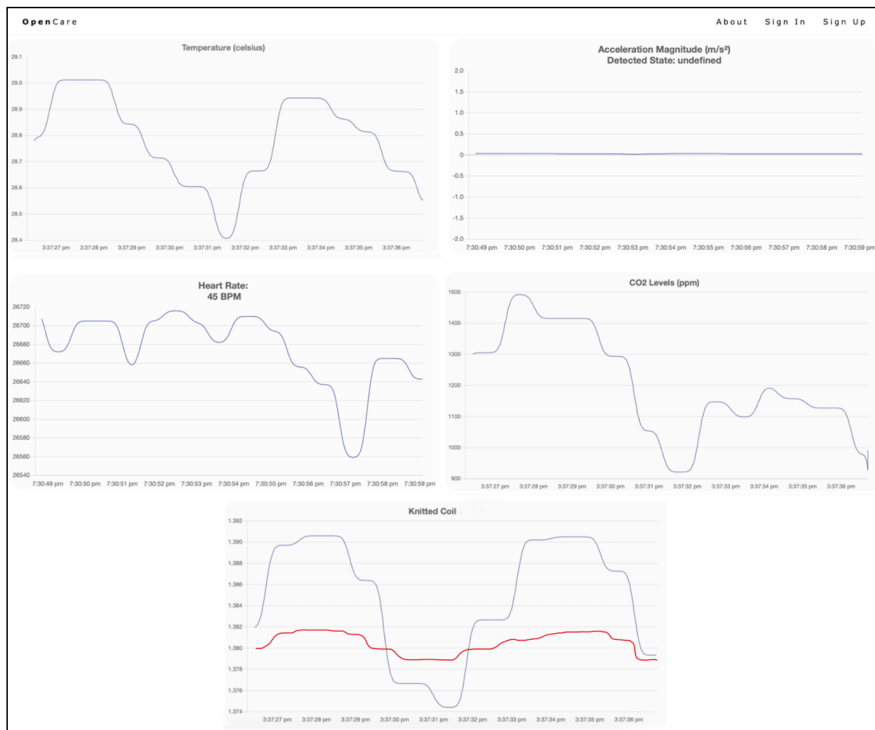


Figure 7.3. Live Data Page

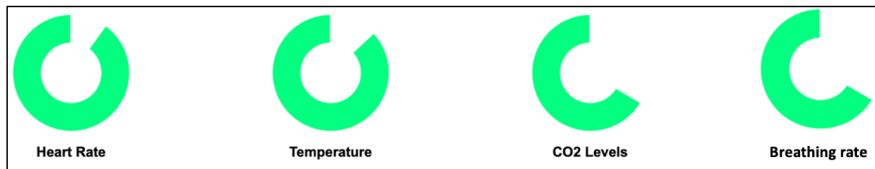


Figure 7.4. Health Indicators

8 Multi-modal data use cases

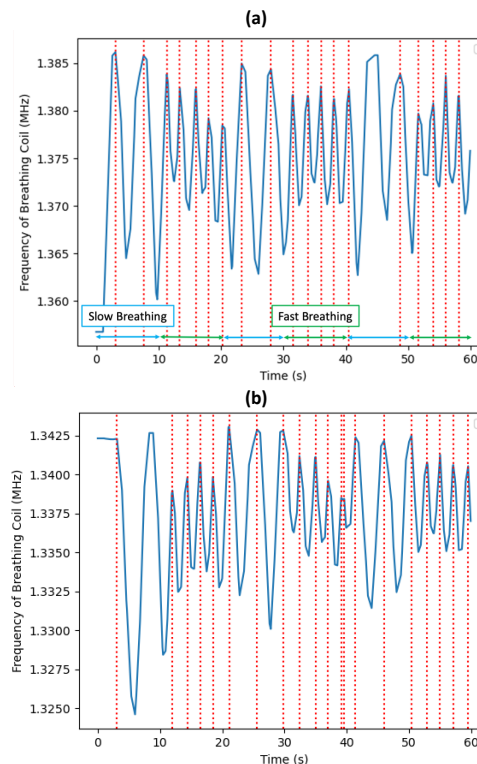
The following section involves the analysis of the multi-modal data that can now be processed and collected with the system we have developed. In Section 8.1, we collect and analyse and collect data solely from the knitted coil and accelerometer. In Sections 8.2 and 8.3, we will explore the relationships between the knitted coil parameters and the mask for both normal and fast breathing scenarios. Finally, in Section 8.4, we will further enhance our understanding of these relationships by employing more complex predictive methods, such as non-linear regression.

8.1 Tracking Respiratory Activity with Knitted Coil

Commented [SM17]: Added all bottom coil data in following figures for this section

Having successfully detected frequency variations in Section 7.3, we can engineer a system to observe changes in breathing rate longitudinally. This key function of the knitted coil emphasizes the importance of extracting breathing rate attributes. We'll validate these tracking techniques by assessing their response to different breathing rates, both rapid and normal. By employing these methods, we can glean deeper insights into respiratory activity than from raw data alone.

Raw Data Measurement



Commented [SM18]: Added labels for fast and normal breathing

Figure 8.1.1. Frequency of Coils with Varying Breathing Rate: (a) Top Coil (b) Bottom Coil

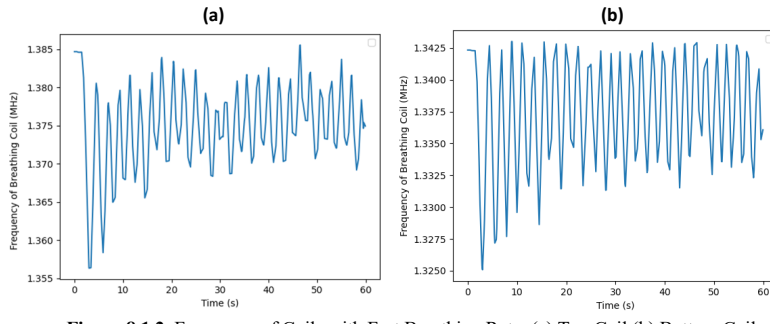


Figure 8.1.2. Frequency of Coils with Fast Breathing Rate: (a) Top Coil (b) Bottom Coil

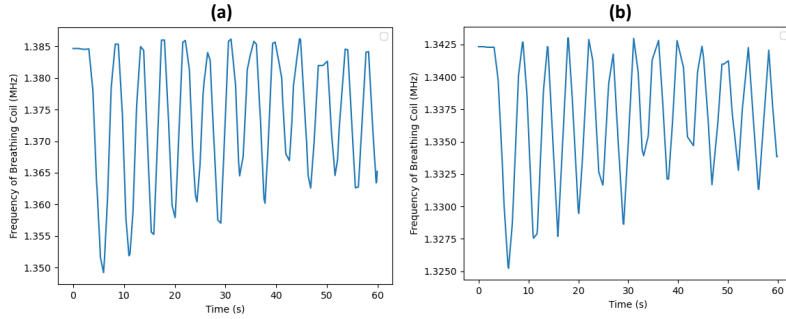


Figure 8.1.3. Frequency of Coils with Normal Breathing Rate: (a) Top Coil (b) Bottom Coil

The initial phase of this procedure involves gathering raw data for analysis. At first, we anticipate a clear shift in the knitted coil's frequency and period correlating with slower or faster breathing rates, but the data reveals more. Notably, changes aren't confined to breathing frequency; they also extend to amplitude alterations, potentially due to incomplete chest muscle contractions during rapid respiration. Subsequently, we'll implement data transformations to accentuate specific data features.

Derivative Measurement

An initial idea was to use the derivative of the raw data collected. We predicted that areas of higher frequencies would similarly yield higher rate of changes.

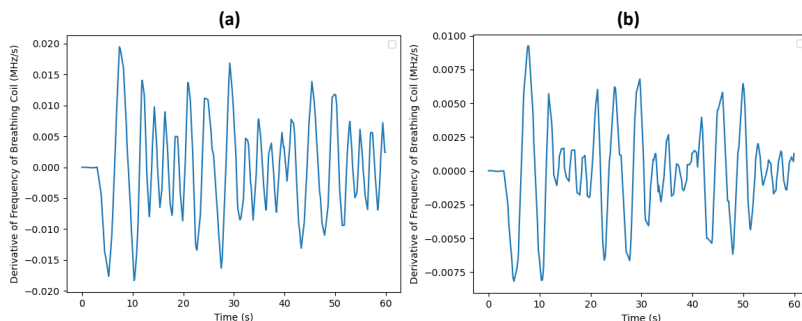


Figure 8.1.4. Derivate of 8.1.1: (a) Top Coil (b) Bottom Coil

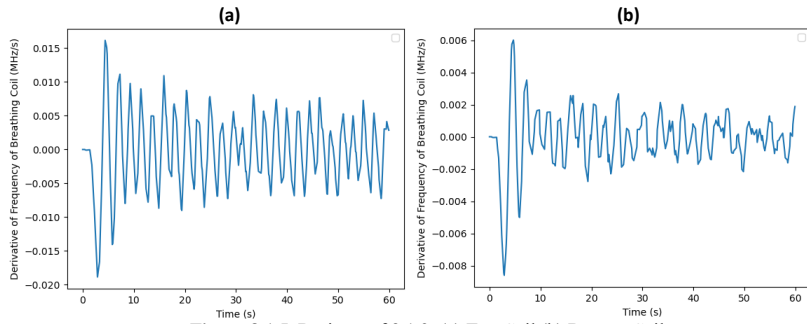


Figure 8.1.5. Derivate of 8.1.2: (a) Top Coil (b) Bottom Coil

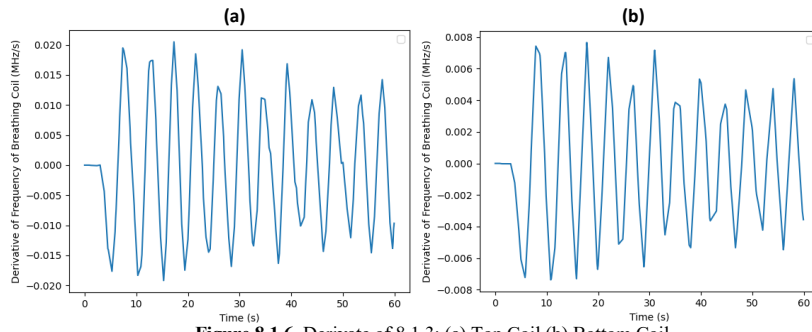


Figure 8.1.6. Derivate of 8.1.3: (a) Top Coil (b) Bottom Coil

Contrary to expectations, the outcomes from Figure 8.1.4 - 8.1.6 revealed lower derivatives during phases of increased breathing rates, vice versa. This unexpected result might be attributed to the homogeneous nature of derivatives (eq. 8.1.7), where both frequency and amplitude influence the resulting derivative, an aspect we hadn't initially considered. This change results in inconsistent results when comparing top and bottom coils, and inconsistent results when comparing fast and normal breathing.

$$(cf(x))' = xf'(x) \quad (8.1.7)$$

Given the inconsistency in the data amplitude, contrary to our initial assumptions, using derivatives as a tracking method for frequency changes is proven to be unreliable. This approach is particularly limited in noisy regions, where minor spikes in variation could lead to significant derivatives.

Sliding Window Peak Counter

We also explored a method involving a 10-second sliding window to count the number of peaks within that timeframe. Unlike the derivative approach, this approach is not only used for tracking frequency, but also provides concrete breathing rate values. Multiplying this count by 6 provides the breathing rate per minute. This technique is anticipated to be more robust, as minor noise fluctuations are less likely to significantly impact the peak count.

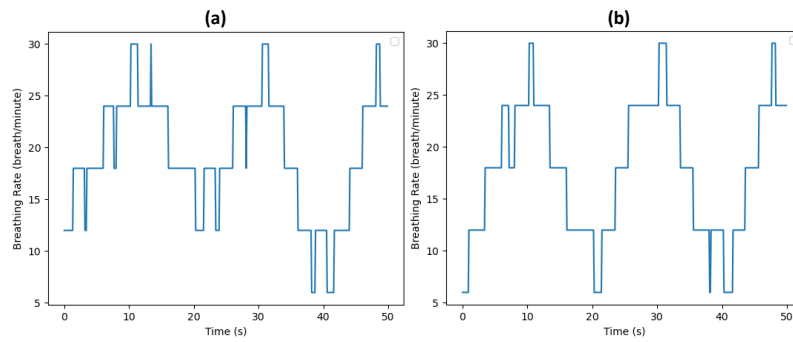


Figure 8.1.8. Sliding Window Applied to 8.1.1: Window Size = 10s: (a) Top Coil (b) Bottom Coil

This method effectively highlighted fluctuations in the breathing rate, demonstrating resistance to amplitude changes and considerable noise immunity: the breathing rate for both top and bottom coil were also very consistent. However, even though its implementation is straightforward, and its performance is reasonable, relying solely on the breathing rate from a sliding window might not provide comprehensive information or adequately represent the complete frequency spectrum.

Short-Time Fourier Transform (STFT)

A final strategy we investigated was the implementation of a Short Time Fourier Transform (STFT). Instead of applying a Fourier Transform to the whole dataset at once, this method uses a smaller window to analyse fragments of data. This technique is anticipated to be not only highly resilient to noise—an attribute that our current sliding window method already possesses—but also capable of capturing the full frequency spectrum. This could potentially supply a broader range of information beyond a single breathing rate value, allowing for more nuanced and accurate data interpretation.

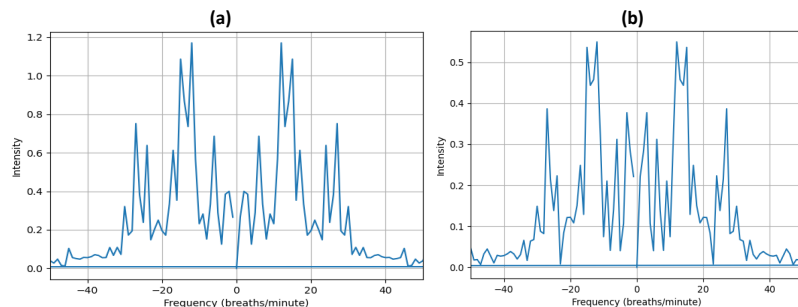


Figure 8.1.9. FFT Applied to 60 seconds range in 8.1.1: (a) Top Coil (b) Bottom Coil

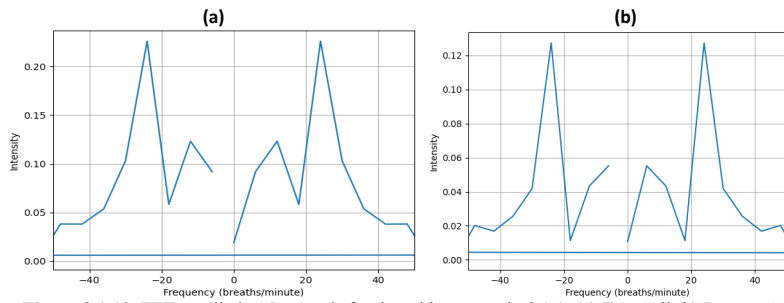


Figure 8.1.10. FTT Applied to 5 seconds fast breathing range in 8.1.1: (a) Top Coil (b) Bottom Coil

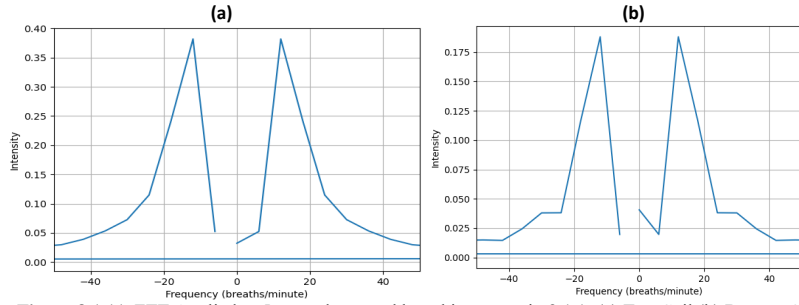


Figure 8.1.11. FTT Applied to 5 seconds normal breathing range in 8.1.1: (a) Top Coil (b) Bottom Coil

Figures 8.1.9 to 8.1.11 display the results derived from applying the STFT technique to various window ranges. These outcomes are corroborated by comparing them with the breathing rate derived from the sliding window approach depicted in Figure 8.1.8. Notably, Figure 8.1.10, reveals the most pronounced frequency component to be around 30 breaths per minute. Figure 8.1.11, shows the dominant frequency component to be approximately 10 breaths per minute. These findings align well with the minimum and maximum breathing rates outlined in Figure 8.1.8, thus demonstrating the accuracy of the method. Furthermore, the resultant transforms for both top and bottom coil only differ by intensity, as expected.

In addition to identifying peak frequency components that correspond to breathing rates, the Short Time Fourier Transform (STFT) could potentially uncover more intricate patterns that wouldn't be discernible by merely considering breaths per minute. A recent study on sleep apnoea detection through machine learning^{xii} revealed a significant correlation with the width and range of frequencies when identifying instances of sleep apnoea. Such values are beyond the capture capability of a rudimentary breathing rate analysis, underscoring the enhanced data interpretation potential of the STFT method.

8.2 Observed Correlations with Normal Breathing

The ensuing section delves into the correlations between the breathing signals obtained by the knitted coils of the knitted coil and health indicators such as temperature, CO₂, accelerometer, and heart rate. This segment is crucial in underscoring the initial observations drawn from the raw data, potentially revealing intriguing associations.

Temperature, CO₂ and Accelerometer Levels

Commented [SM19]: Added accelerometer data for section

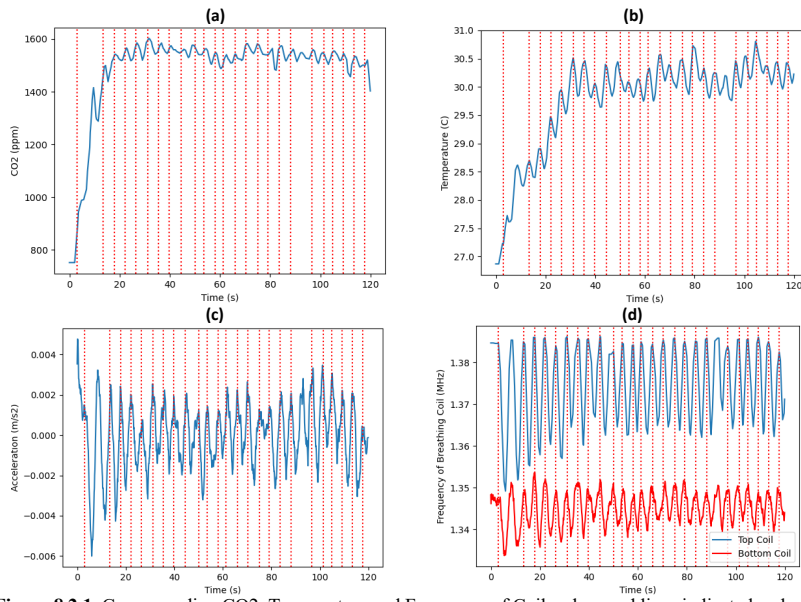


Figure 8.2.1. Corresponding CO₂, Temperature and Frequency of Coils where red lines indicate local maxima:
 (a) CO₂ (b) Temperature (c) Accelerometer L2 Norm (d) Frequency of Coils

We note that temperature, CO₂, acceleration, and frequency all appear to be nearly in phase. Figure 8.2.1 demonstrates this relationship, showing that when the local maxima for frequency are superimposed on the other time series plots, the peak values for the other graphs align closely. Another finding is the similar settling times exhibited by both sensors, approximately 30 seconds, which is the time required to transition from room values to breath values.

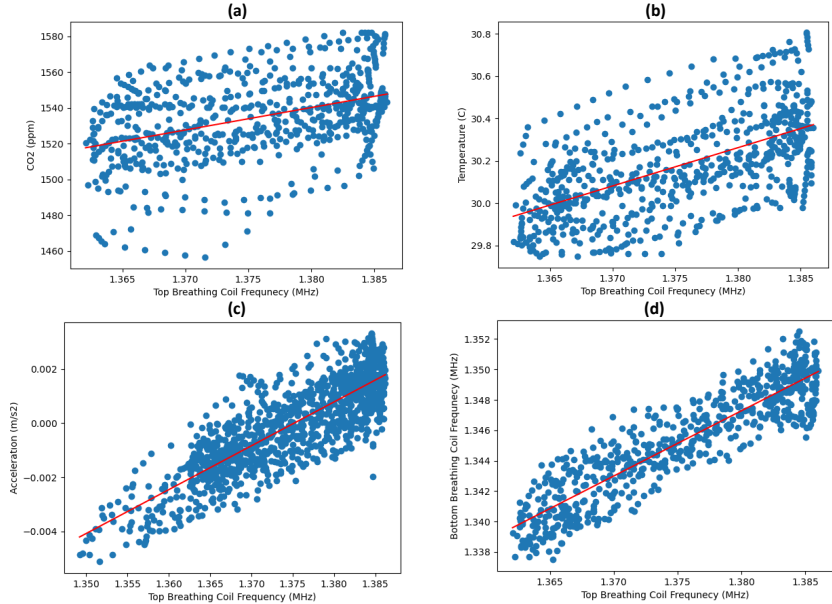


Figure 8.2.2. (a) Top Breathing Coil Frequency against CO2 (b) Top Breathing Coil Frequency against Temperature (c) Top Breathing Coil Frequency against Accelerometer L2 Norm (d) Top Breathing Coil Frequency against Bottom Breathing Coil

Upon further observation, strong correlation coefficients were found between the top breathing coil and the bottom breathing coil (0.91), as well as the top breathing coil and the accelerometer L2 norm (0.87). However, weaker correlation coefficients of 0.42 and 0.59 were observed for the top breathing coil against CO2 and Temperature, respectively. We suspect that the presence of outliers, noise, and non-linearity in the correlation may have contributed to this weak correlation. Therefore, these coefficients may underestimate the true relationship between the variables. On the other hand, accelerometer, and bottom breathing coil, which both utilize chest movement to obtain values, are less susceptible to noise in controlled conditions. To address these limitations for CO2 and temperature and uncover non-linear relationships, we could leverage Machine Learning techniques in the subsequent sections.

Heart Rate

An observation we noted regarding heart rate involved minor fluctuations in the rate during the phases of inhalation and exhalation. Subsequent research confirmed the existence of a relationship between heart rate and breathing state known as Respiratory Sinus Arrhythmia (RSA). RSA is characterized by the modulation of premotor cardioinhibitory parasympathetic neuron (CPN) activity^{xlii}, corroborating our initial observation.

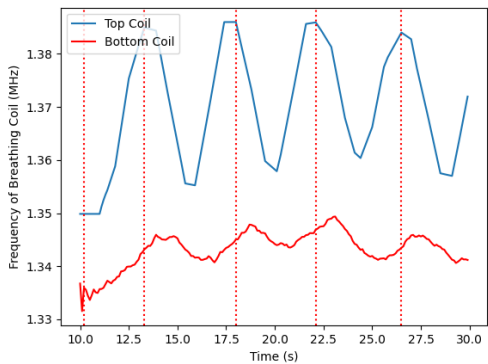


Figure 8.2.3. Breathing Signals from Top and Bottom Coil

Commented [SM20]: Added bottom coil values

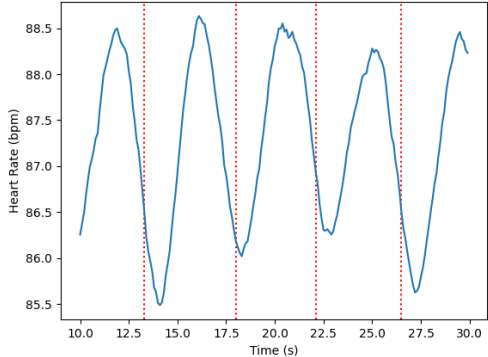


Figure 8.2.4. Extracted Heart Rate from the PPG sensor on the cheek measured simultaneously with figure 8.2.3

It is noticeable that the periods of the fluctuations of top coil, bottom coil and heart rate is quite similar; however, they all have slightly different phases. Based on our research^{xlii}, we anticipate a 180-degree phase shift, given that our frequency peaks during exhalation, which should align with a decreased heart rate. Nevertheless, a slight delay, resulting in a phase shift marginally over 180 degrees, might be attributable to the application of a moving average filter or potential sensor delays. Moreover, certain studies on the phase differences between heart rate and respiration^{xliii} assert that "heart rate and breathing are not always in phase during resonant frequency breathing."

8.3 Observed Correlations with Fast Breathing

The findings presented in section 8.2 demonstrate discernible relationships between chest diameter and breathing parameters. In an ideal scenario, these relationships should remain consistent even during rapid breathing. However, due to mask sensor limitations, we anticipate a slightly reduced correlation in cases of fast breathing, which might be attributed to delays in CO₂ and temperature sensor responses.

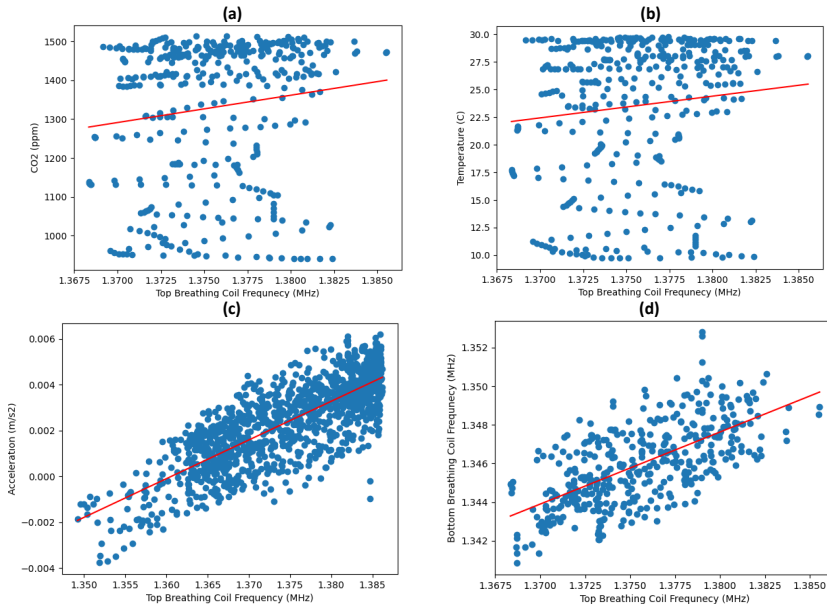


Figure 8.3.1. (a) Top Breathing Coil Frequency against CO₂ (b) Top Breathing Coil Frequency against Temperature (c) Top Breathing Coil Frequency against Bottom Breathing Coil

The frequencies of the top and bottom breathing coils exhibit a strong correlation (0.82), as do the frequencies of the top breathing coil and acceleration (0.83). However, the correlations between the coil frequencies and both temperature and CO₂ are considerably weaker, measuring at 0.21 and 0.13 respectively.

This weaker correlation can be attributed to the operating mechanism of the temperature and CO₂ breath sensors. These sensors heat up when breathed on and gradually cool down in the absence of breath, returning to room temperature values. Due to their response time, during periods of rapid breathing, these sensors may not react quickly enough to capture the changes, resulting in a negligible correlation being observed.

Upon further investigation, we observed that the correlation between the top breathing coil and accelerometer barely decreased. This could be because fast breathing, which initially seemed to introduce inaccuracies, lead to higher accelerometer changes, resulting in a higher signal-to-noise ratio (SNR), as we discovered in section 5.2.

Additionally, we uncovered that the reduction in correlation for frequency could potentially be attributed to phase differences. To explore this, we employed an algorithm that looped through a range of delays, computed the correlation for each delay and found the delay with the maximum correlation. We found that at a delay of 0.82 seconds, the correlation was maximized at 0.87.

Commented [SM21]: made a peak correlation finder and found an increase in correlation when adding a shift of 82 index or 0.82 seconds on the array

8.4 Performance of Predictive Models

Given the weak correlation between chest movement and both CO₂ levels and temperature, we plan to design and implement machine learning techniques—including outlier removal, linear regression, and nonlinear regression—to determine whether the low correlation is merely a consequence of nonlinearity and outliers. Moreover, these models could eventually be leveraged to predict breath CO₂ and temperature levels solely using the knitted coils. As for the heart rate and accelerometer, since we've already established a strong relationship, and it's impractical and it's easy to obtain these values by placing these sensors in body areas, no predictive models will be designed for it. Considering the lack of correlation with fast breathing due to sensor limitations, the predictive models will solely be examined in the context of normal breathing.

Linear Regression

An initial least square regression model (eq. 8.4.1) where A was training frequency, b was predicted outcome, and x were the parameters, provided the best fit in figure 8.4.2 and 8.4.3. The process of training and testing involved taking 2 minutes of data, the first 1.5 minutes would be used to obtain the parameters and the last 0.5 minutes to test the results.

$$Ax = b$$

$$x = (A^T A)^{-1} A^T b \quad (8.4.1)$$

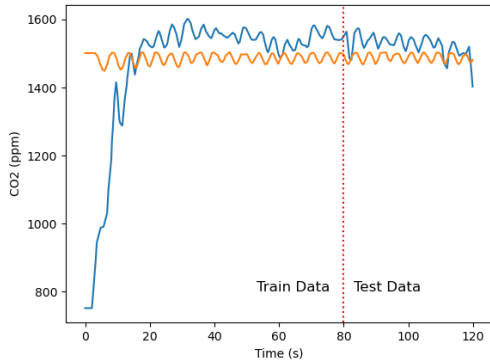


Figure 8.4.2. Using Linear Regression to Predict CO₂ Levels: Blue – Actual, Orange – Predicted

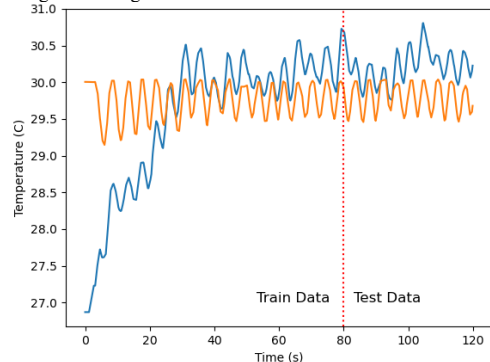


Figure 8.4.3. Using Linear Regression to Predict Temperature Levels: Blue – Actual, Orange – Predicted

	Mean Bias	Mean Absolute Error	Mean Squared Error	Mean Absolute Percentage Error (%)
CO2 Predictions	-38.65	40.81	2039.64	2.66
Temperature Predictions	-0.43	0.43	0.23	1.42

Table 8.4.4. Performance of Predictors

Observations from Table 8.4.4 and Figures 8.4.2 and 8.4.3 primarily highlighted the presence of negative mean biases. This phenomenon is likely a result of the initial 'logistic phase' contributing a negative skew to the data. Addressing this issue could involve two potential strategies: manually eliminating outliers or employing an algorithm such as RANSAC^{xliv}, or alternatively fitting a logistic model to the training data before its removal, thereby aligning the remaining data more closely with our expectations.

- 1:** For K iterations
 - 2:** Select random samples
 - 3:** Fit a model
 - 4:** Check how many samples are inliers
 - 5:** Terminate after a certain number of iterations or inliers have been found

Algorithm 8.4.5. RANSAC Outlier Removal Algorithm

Applying the RANSAC algorithm outlined in Algorithm 8.4.5 removed most of the outlier data that we expected (early converging data).

	Mean Bias	Mean Absolute Error	Mean Squared Error	Mean Absolute Percentage Error (%)
CO2 Predictions	8.38	17.885	619.735	1.185
Temperature Predictions	-0.036	0.153	0.038	0.506

Table 8.4.6. Performance of Predictors

As expected, after the removal of outliers the overall performances shown in Table 8.4.6 shows large improvements and no longer has a glaring mean bias.

Logistic – Linear Regression

The following procedure that could be used to obtain a better model and predict values during convergence periods would be to add a logistic function. The final parameters of the model could be the slope and intercepts used in Linear Regression alongside the logistic function parameters^{xlv}:

$$y = mx + b + \left[\frac{L}{1 + e^{-k(t-x_0)}} + b' \right] \quad (8.4.7)$$

The first step would be to fit the logistic function parameters to obtain the parameters for a logistic function dependent on time:

$$\text{logistic_fit}(t) \quad (8.4.8)$$

After doing this, we could normalize all the y using the logistic function, and train on the normalized data, y' :

$$y' = y - \text{logistic_fit}(t) \quad (8.4.9)$$

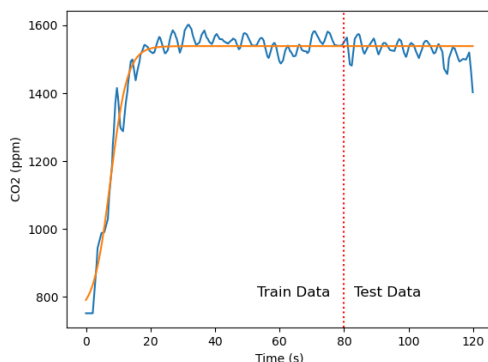


Figure 8.4.10. Logistic Fit of CO2: Blue – Actual, Orange – Predicted

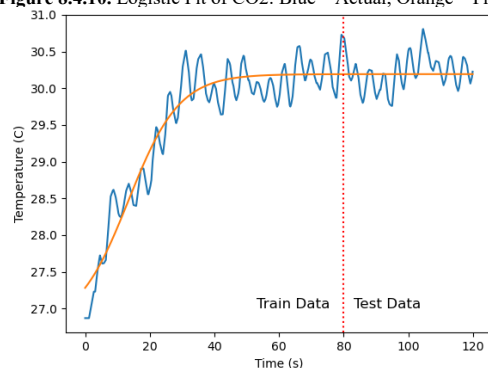


Figure 8.4.11. Logistic Fit of Temperature: Blue – Actual, Orange – Predicted

The values were fit using the Lavenberg-Marquardt^{xlvii} algorithm and gave fits shown in Figure 8.4.10 and Figure 8.4.11. Following this, we can apply normalization to the data (eq. 8.4.9) then use a linear regression and evaluate the new performance.

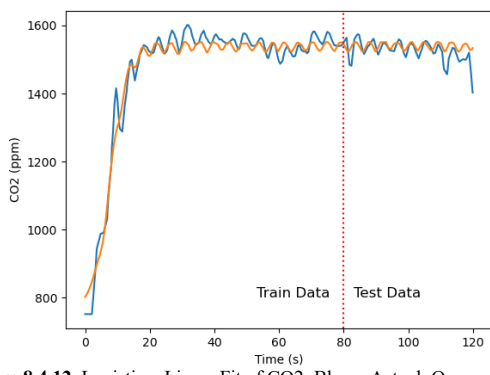


Figure 8.4.12. Logistic – Linear Fit of CO2: Blue – Actual, Orange – Predicted

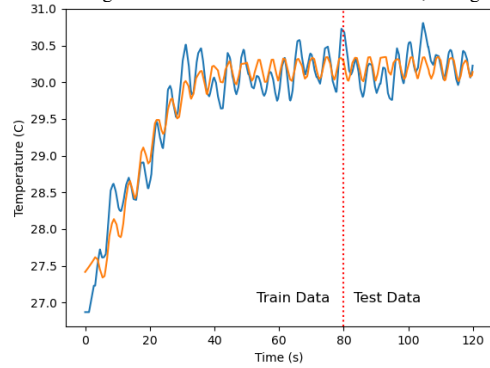


Figure 8.4.13. Logistic – Linear Fit of Temperature: Blue – Actual, Orange – Predicted

After applying training, the model with linear regression on the normalized data then applying the final Logistic – Linear Fit (eq. 8.4.7) we obtained the predicted values shown in Figure 8.4.12 and 8.4.13.

	Mean Bias	Mean Absolute Error	Mean Squared Error	Mean Absolute Percentage Error (%)
CO2 Predictions	12.379	19.608	706.283	1.301
Temperature Predictions	-0.012	0.150	0.037	0.495

Table 8.4.14. Performance of Predictors

The Logistic – Linear model performed slightly better, across the board, compared to the outlier adjusted values in 8.4.6 in terms of temperature and slightly more poorly in terms of CO2.

8.5 Conclusion

This section's analysis confirms a significant correlation between health parameters—such as breath CO₂ and temperature, and heart rate—and variations in chest and abdomen diameter. We effectively demonstrated how the initial correlation coefficient, computed in section 8.2, underestimated the data's relationship. By employing non-linear models and outlier removal, we could reveal a stronger association than previously deduced. Furthermore, this section emphasizes the limitations and challenges of depending solely on facial sensors for breath tracking. During instances of rapid breathing, as detailed in section 8.3, these sensors struggled to react promptly to temperature and CO₂ changes, resulting in a substantially limited correlation: this observation is supported by earlier literature research ^{xv}, where it explained that directly measure chest diameter changes is much more accurate as it is directly affected by respiration compared to temperature and CO₂ changes which are indirectly affected by respiration. This discrepancy further accentuates the advantages of the knitted coil, which provides a more immediate and robust method for breath monitoring. As indicated in section 8.1, the knitted coil proved highly effective at detecting minute changes in breathing rate and supplying comprehensive frequency spectrums with minimal noise after the appropriate transformations. This suggests that the knitted coil may present a superior alternative for tracking and analysing breathing patterns.

This section's findings also offer valuable insights for future research directions. Firstly, the Short Time Fourier Transform (STFT) features of the knitted coil have proven to be highly effective in tracking breathing patterns. Therefore, when investigating the impact of pure breathing patterns on health, these STFT features could serve as the foundation for the most reliable models. Secondly, the knitted coil has shown potential in predicting the CO₂ and temperature of breaths, albeit with limited reliability during episodes of rapid breathing this suggests that the knitted coil could be integrated with existing systems which expect CO₂ and temperature inputs. Lastly, we've demonstrated a potent relationship between the knitted coil and several key health parameters commonly employed in training models used to detect respiratory conditions. Given the substantial correlations between the knitted coil and these parameters, it suggests the viability of future studies to focus on utilizing knitted coils to predict these respiratory conditions. Therefore, the knitted coil can be seen as a promising tool in advancing respiratory health research and technology.

9 Future Work

This subsequent section emphasizes potential avenues for expanding upon the outcomes of this project. Initially, we will address prospective upgrades to the functionality and reliability of the mask and knitted coil for a second iteration. Subsequently, we will discuss enhancements and updates for the application interface. Lastly, we will examine advancements concerning research into respiratory diseases and the utilization of big data analytics.

9.1 Improvements to the Functionality and Form of the Mask and Knitted Coil Hardware

While current version of our mask and knitted coil offers decent functionality and convenient form factors, several improvements can still be made when looking to develop a future version in terms of functionality and form factor.

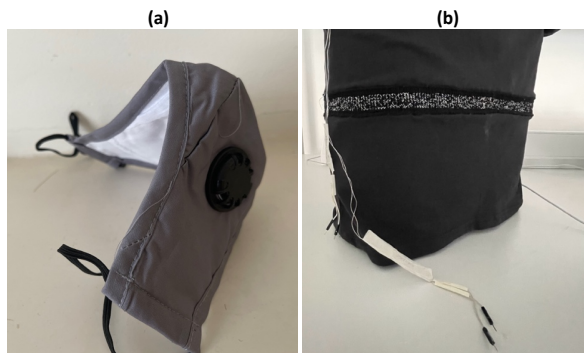


Figure 9.1.1. (a) Smart Breathing Mask (b) Knitted Coil

	Smart Mask V1	Knitted Coil
Health Parameters Provided	Heart Rate, Movement, CO ₂ , Temperature	Chest Diameter Changes
Bluetooth	Yes	No
Wi-Fi	Yes	Yes
Weight	60g	80g
Budget	MAX30102 - £3 Si7021 - £10 CCS811 - £10 MPU6050 - £10 ESP32 - £3 Battery - £5 Mask - £5 Total: £46	ESP32 - £3 Insulated Technical Wire - £5 Yarn - £5 Coils and Shirt - £9 Battery - £5 Total: -£27
Battery Life	6 hours	10 hours
Rechargeable	No	No
Exposed Sensors/Wiring	Yes	Yes

Table 9.1.2. Device Specifications

Figure 9.1.1 depicts the present prototypes for our devices, while Table 9.1.2 provides a detailed account of the devices' specifications.

Improving Functionality

In terms of augmenting functionality, there are multiple avenues to consider. One such approach is to maximize the utility of existing sensors, such as the blood oxygen sensor in the MAX30102, the air humidity sensor in the Si7021, and the air quality sensor in the CCS811. Such an initiative would not entail additional costs and would have an imperceptible impact on battery life and processing speed. Furthermore, we could introduce new sensors like the particle sensor discussed in Section 4.4, which would provide further data to refine the models being created.

Improving Power Management

The current device is powered via the micro-USB port using a power bank with a voltage of 5V, a current of 2A, and a capacity of 5000mAh. Because the ESP32 relies heavily on the Wi-Fi and Bluetooth modules for communication, it is estimated to consume around 800mA when active. With this implementation, the device has an estimated battery life of 6.25 hours when operating continuously.

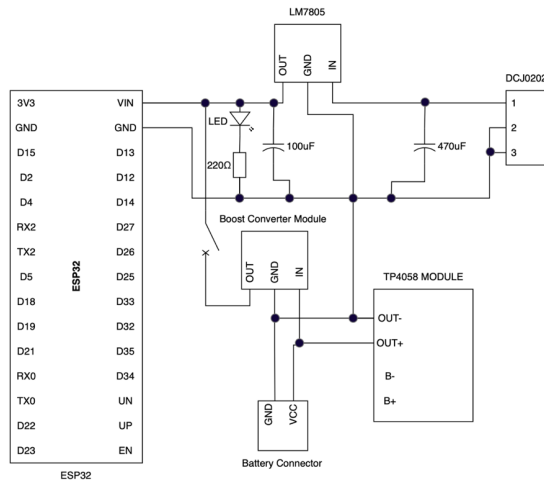


Figure 5.2.4. Proposed Battery Configuration Design take from ^{xlvii}

Commented [SM22]: added battery config into the future work

Although convenient for early use, the battery configuration with a power bank has portability, flexibility, efficiency, and cost issues, therefore the configuration using a lithium-ion battery and a step-up boost converter (shown in Figure 5.2.4) could be used in the final design.

9.2 Improvements to Application Interface

Apart from advancements to the hardware and form factor, numerous enhancements can be made to the application interface of the device, greatly improving user interaction and experience.

The first point of improvement is the implementation of a more intuitive and user-friendly interface. The UI can be simplified and made more engaging by using recognizable icons, less technical jargon, and more visual representations of data. For instance, data visualization techniques such as graphs and charts can be incorporated to display information in a more understandable and accessible manner.

Secondly, personalization features can be introduced to cater to the individual needs and preferences of each user. This may involve allowing users to customize the interface, from colour schemes and font sizes to dashboard layout. This not only promotes a sense of ownership but also enhances ease of use. Thirdly, the integration of a more comprehensive tutorial or help system would significantly improve the user experience. Users should be able to understand how to navigate the application and troubleshoot common issues without needing to reach out to support. This might include interactive guides, FAQ sections, and tooltips.

Moreover, real-time feedback and alerts can be employed to notify users of important changes in the recorded data. Push notifications or alarms can be programmed to alert users when specific thresholds are breached. This ensures the user is kept up to date with their health status and can take timely action when necessary.

Lastly, the app interface can also be improved by introducing features that enable data sharing and integration with other health apps. This can help users better understand their overall health, by correlating respiratory data with other health indicators.

These proposed improvements would make the application interface more engaging, intuitive, and user-friendly, thereby enhancing user satisfaction and overall interaction with the device.

9.3 Progression in Research and Utilization of Big Data Analytics

Exploration and Integration on Developed and Researched Models

Instead of focusing on training and developing new models and algorithms, several systems have already been created with open-source software available for public use. These models have been heavily trained and tested with large datasets which infer robustness and reliability.

A current model under scrutiny for its potential in diabetes detection is the XGBoost Algorithm^{xxviii}. This research investigates the use of temperature and CO₂ sensors for analysing characteristics of exhaled breath. Typically, diabetic patients lack sufficient insulin to metabolize glucose for energy, leading to fat breakdown and resultant ketone production^{xvii}. Acetone, one of these ketones, is expelled through breath, influencing exhaled CO₂ levels. Additionally, diabetes can damage blood vessels, potentially affecting circulation and, indirectly, the temperature of breath.

Several models, including Support Vector Machines (SVM), Deep Neural Networks (DNN), and Convolutional Neural Networks (CNN), were tested in the study. Over 100 patients' data were employed to train these models, generating impressive accuracy and recall rates of 99% and 100%, respectively.

Our knitted coil and mask could be easily integrated with this developed model, by providing predicted and actual CO₂ and temperature of breath as inputs for these models. Furthermore, the use of our knitted coil could offer enhancements to the model by also considering the respiratory rate, as high blood sugar levels often lead to dehydration, subsequently affecting typical respiratory rates. As demonstrated in previous sections, the knitted coil exhibits exceptional precision and robustness in tracking respiratory rates, offering an advantage over CO₂ and temperature measures, which underperform to track high respiratory rates.

Research and Development into Underdeveloped Areas

As an alternative to relying solely on established and researched models, it could be valuable to delve deeper into relatively unexplored areas. These undertakings might lead to the identification of novel correlations and insights. One such area, as previously mentioned, involves examining the relationship between shifting frequency domains in Short-Time Fourier Transform (STFT) and various respiratory diseases.

While a significant body of research has been conducted on the association between respiratory rate and health conditions, the in-depth analysis provided by STFT remains largely unexplored. This approach, which delves into the intricate, nuanced frequency alterations over time, may yield more complex and previously uncharted relationships.

Expanding our investigation into these areas not only has the potential to enhance our understanding of respiratory health, but also helps in refining our analytical models. By integrating these less explored yet potentially rich data sources, we can ensure a more comprehensive, precise, and predictive model. The discovery of novel relationships could ultimately lead to breakthroughs in early disease detection and more effective patient care strategies.

10 Conclusion

This conclusion section will focus on evaluating the success and challenges faced of the project based on the defined evaluation metrics in section 3.4, then focus on summarizing the highlights and discoveries found during this project.

10.1 Evaluating Success

Objective 1: Create a smart mask sensor system based on multiple commercial sensors considering factors such as effectiveness, reliability, and accuracy

Objective 1 was executed quite well. Comprehensive literature research on all the sensors for the ESP32 was carried out, leading to successful data procurement. Initial impediments emerged with the 0.25 second delay brought about by the CCS811 sensor, which inadvertently spread to other sensors. This hurdle was tackled successfully by implementing multithreading, thereby ensuring uninterrupted processes from each sensor. After corroborating the correct functioning of all sensors, we transitioned from a breadboard setup to a more compact arrangement that seamlessly fit within the mask chassis.

Objective 2: Implement a multimodal sensor system based around the ESP32, ensuring seamless integration of various sensor inputs (including the smart mask sensor system and knitted RIP coil sensor) with a server and efficient data processing capabilities

Objective 2 was also accomplished with minor challenges. We successfully constructed the data processing features, including the pan-Tompkins algorithm, and smoothly integrated data transfer from the ESP32 to the test server with virtually no issues.

Objective 3: Create an intuitive and user-friendly environment to interact with and display mask sensor and knitted RIP data. The environment should include a web-based interface which supports real-time monitoring, data visualization and data export functionalities

We met some challenges during Objective 3, specifically regarding the design and implementation due to our limited web development experience. However, we overcame these obstacles by leveraging available resources. The end result was a fully functional, web-based interface that showcased a high degree of effectiveness, as illustrated in section 7.

Objective 4: Using the created environment, conduct comprehensive analysis to determine correlations and relationships between the data obtained from the smart breathing mask and knitted RIP

Objective 4 presented some initial setbacks, specifically in deriving useful data from the knitted RIP, which we thoroughly discussed in section 6. With iterative experimentation, we managed to harness valuable insights using the ESP32. While the analysis did encounter a few missteps, such as deriving frequency via derivative, further trials led to the extraction of valuable data and meaningful correlations.

Objective 5: Conduct a thorough evaluation of potential research directions and applications for the smart mask sensor system and multimodal sensor systems.

The majority of Objective 5 was encapsulated in the future work section in section 9. Although the trajectory of this research is yet to be fully substantiated, I believe the work thus far has been executed with ample depth and detail.

Commented [SM23]: Revisited evaluation in beginning and summarised the challenges faced and success

10.2 Summary

Commented [SM24]: Summarized all work

All in all, each objective was accomplished adeptly within the given timeline, covering research, mask design, knitted RIP's integration into the IoT system, front-end software design, and data analysis.

In the realm of research, as detailed in section 4, we undertook an exhaustive exploration of this research field's significance. Intriguingly, we discovered that the use of garments in the current health technology industry was quite limited, indicating an untapped growth potential. Furthermore, we stumbled upon compelling methodologies for tracking breathing, such as infrared cameras, and innovative approaches to air filtration, including a responsive mask that sprays in reaction to airborne pathogens.

With regards to the mask's design and analysis, featured in section 5, we successfully engineered a functional mask capable of providing live readings and monitoring four crucial health parameters. Through rigorous testing, we established that the CO₂, temperature, and acceleration sensors yielded a robust response to breath when correctly positioned. Additionally, we evaluated heart rate consistency, comparing our results with industry-standard devices like the Apple Watch.

Concerning the integration of the knitted RIP into our multi-modal system, as discussed in section 6, we achieved this seamlessly. We ensured that the data could be interpreted by an ESP32 and transmitted to a server via HTTP.

As for the creation of an interactive front-end detailed in section 7, we prioritized intuitive user experience and ease of use. We also designed the software to be scalable, making it suitable for potential mass production in the future.

Lastly, in the context of data analysis, illustrated in section 8, we unearthed intriguing and unexpected correlations, such as the one between heart rate and breathing. Additionally, we noted that the CO₂, temperature, and acceleration readings exhibited similar patterns to the top and bottom coil of the knitted RIP. By leveraging regression techniques, we managed to reveal complex nonlinear relationships, further strengthening the interconnectedness of these variables.

11 Appendix

Ethical, Legal and Safety Plan

This project involves a hardware-based approach that requires frequent interaction with electrical components. In addition, the project focuses on the health technology sector, which necessitates the regular analysis of user data. Given these considerations, it is crucial to establish a comprehensive ethical, legal, and safety plan to guide the project's design and development, however since this project is currently in its initial development phase, no testing will be conducted with volunteers at this stage. The following guidelines outline important considerations that must be addressed to ensure that the project is safe, legal, and ethical throughout its progression.

Ethical

1. Respect user privacy and ensure that user data is always protected, such as by using encryption methods to secure user data.
2. Obtain informed consent from users before collecting and analysing their health information and provide clear and concise information about the purpose of collecting user health information.
3. Ensure that the device is not used to discriminate against individuals based on their health status and take appropriate measures to prevent such discrimination.
4. Regularly review and update the ethical plan to ensure that it reflects the evolving ethical considerations related to the use of the device.

Legal

1. Ensure that the device complies with all applicable laws and regulations, such as data protection laws and health information privacy laws, such as the EU's General Data Protection Regulation (GDPR) ^{xlix}.
2. Obtain any necessary licenses or permits for the design, manufacture, and sale of the device, and ensure that the device meets all applicable safety standards.
3. Protect any intellectual property associated with the device, such as patents, trademarks, and copyrights.

Safety

1. Test the device thoroughly and safely to ensure that it functions properly and does not pose a risk to users or testers, and regularly conduct safety assessments to identify and mitigate any potential safety risks. These include reviewing the wiring, ensuring limited exposure to electrical components, and verifying that the device is properly grounded.
2. Provide clear and concise instructions for users on how to properly use and maintain the device and include appropriate warning labels on the device to alert users to any potential safety hazards. These could typically include hazards to swallowing small electrical components, exposed wiring or electrical shocks from live wires or improper grounding.
3. For safe wireless communication, adhere to safety protocols such as ensuring devices are within regulated limits like the FCC's radio frequency exposure limit of 1.6 watts/kg . Additionally, maintain a safe distance from transmitting antennas, use protective gear when required, and follow manufacturer guidelines for proper device usage and maintenance.

- ⁱ Fobelets, K. (2020). Knitted coils as breathing sensors. Sensors and Actuators A: Physical, 306, 111945. <https://doi.org/10.1016/j.sna.2020.111945>
- ⁱⁱ Adeel, M., Cotur, Y., Naik, A., Gonzalez-Macia, L., & Güder, F. (2022). Face masks as a platform for wearable sensors. Nature Electronics. <https://doi.org/10.1038/s41928-022-00871-2>
- ⁱⁱⁱ Andrea Coravos, Jennifer C. Goldsack, Daniel R. Karlin, Camille Nebeker, Eric Perakslis, Noah Zimmerman, M. Kelley Erb; Digital Medicine: A Primer on Measurement. *Digit Biomark* 5 September 2019; 3 (2): 31–71. <https://doi.org/10.1159/000500413>
- ^{iv} The Guardian. (2018, June 1). Cancer patients could be saved by 'Fitbits for the tumour'. <https://www.theguardian.com/technology/2018/jun/01/cancer-fitbit-treatment-chemotherapy>
- ^v Dunn J, Runge R, Snyder M. Wearables and the medical revolution. *Per Med*. 2018 Sep;15(5):429-448. doi: 10.2217/pme-2018-0044. Epub 2018 Sep 27. PMID: 30259801.
- ^{vi} <https://support.apple.com/en-gb/guide/watch/apd2054d0d5b/watchos>
- ^{vii} Reeder B, David A. Health at hand: A systematic review of smart watch uses for health and wellness. *J Biomed Inform*. 2016 Oct;63:269-276. doi: 10.1016/j.jbi.2016.09.001. Epub 2016 Sep 6. PMID: 27612974.
- ^{viii} <https://www.smartstringnews.com/posts/motiv-vs-oura-ring-which-is-the-best-sleep-and-activity-tracking-smart-ring>
- ^{ix} NHS Inform. (n.d.). Illnesses and conditions - Lungs and Airways. <https://www.nhsinform.scot/illnesses-and-conditions/lungs-and-airways>
- ^x Chen, A., Zhang, J., Zhao, L., Rhoades, R. D., Kim, D. Y., Wu, N., Liang, J., & Chae, J. (2020). Machine-learning enabled wireless wearable sensors to study individuality of respiratory behaviors. *Biosens Bioelectron*, 173, 112799. <https://doi.org/10.1016/j.bios.2020.112799>
- ^{xi} Tsang, K. C. H., Pinnock, H., Wilson, A. M., & Shah, S. A. (2022). Application of Machine Learning Algorithms for Asthma Management with mHealth: A Clinical Review. *J Asthma Allergy*, 15, 855-873. <https://doi.org/10.2147/JAA.S285742>
- ^{xii} McDowell, A., Kang, J., Yang, J., Jung, J., Oh, Y.-M., Kym, S.-M., Shin, T.-S., Kim, T.-B., Jee, Y.-K., & Kim, Y.-K. (2022). Machine-learning algorithms for asthma, COPD, and lung cancer risk assessment using circulating microbial extracellular vesicle data and their application to assess dietary effects. 30 September 2022.
- ^{xiii} National Health Service. (n.d.). Spirometry. Retrieved June 23, 2023, from <https://www.nhs.uk/conditions/spirometry/>
- ^{xiv} Pereira, C. B., Yu, X., Czaplik, M., Rossaint, R., Blazek, V., & Leonhardt, S. (2017). Remote monitoring of breathing dynamics using infrared thermography. *Biomedical Optics Express*, 8(11), 4838-4850. <https://doi.org/10.1364/BOE.8.004838>
- ^{xv} Retory Y, Niedzialkowski P, de Picciotto C, Bonay M, Petitjean M. New Respiratory Inductive Plethysmography (RIP) Method for Evaluating Ventilatory Adaptation during Mild Physical Activities. *PLoS One*. 2016 Mar 23;11(3):e0151983. doi: 10.1371/journal.pone.0151983.
- ^{xvi} Li, J., Yin, J., Ramakrishna, S., & Ji, D. (2023). Smart Mask as Wearable for Post-Pandemic Personal Healthcare. *Biosensors*, 13, 205. <https://doi.org/10.3390/bios13020205>
- ^{xvii} Kalavakonda RR, Masna NVR, Mandal S, Bhunia S. A smart mask for active defense against airborne pathogens. *Sci Rep*. 2021 Oct 7;11(1):19910. doi: 10.1038/s41598-021-99150-x.
- ^{xviii} Akduman, C., and Akçakoca Kumbasar, E. P. "Nanofibers in Face Masks and Respirators to Provide Better Protection." *IOP Conference Series: Materials Science and Engineering*, vol. 460, 2018, p. 012013. iopscience.iop.org/article/10.1088/1757-899X/460/1/012013/pdf
- ^{xix} Hyysalo, J., Dasanayake, S., Hannu, J., Schuss, C., Rajanen, M., Leppänen, T., Doermann, D., & Sauvola, J. (2022). Smart mask – Wearable IoT solution for improved protection and personal health. *Internet of Things*, 18, 100511. <https://doi.org/10.1016/j.iot.2022.100511>
- ^{xx} Maxim Integrated Products. (2019, October 29). MAX30102 Datasheet. <https://www.analog.com/media/en/technical-documentation/data-sheets/MAX30102.pdf>
- ^{xxi} Budidha, K., & Kyriacou, P. A. (2019). Photoplethysmography for Quantitative Assessment of Sympathetic Nerve Activity (SNA) During Cold Stress. *Frontiers in Physiology*, 10, 1863. <https://doi.org/10.3389/fphys.2018.01863>

- ^{xxii} Esgalhado, F.; Batista, A.; Vassilenko, V.; Russo, S.; Ortigueira, M. Peak Detection and HRV Feature Evaluation on ECG and PPG Signals. *Symmetry* **2022**, *14*, 1139. <https://doi.org/10.3390/sym14061139>
- ^{xxiii} Hartmann, V., Liu, H., Chen, F., Hong, W., Hughes, S., & Zheng, D. (2019). Toward Accurate Extraction of Respiratory Frequency From the Photoplethysmogram: Effect of Measurement Site. DOI:[10.3389/fphys.2019.00732](https://doi.org/10.3389/fphys.2019.00732)
- ^{xxiv} Advanced Manufacturing Services. (2016, December 23). CCS811 Datasheet. https://cdn.sparkfun.com/assets/learn_tutorials/1/4/3/CCS811_Datasheet-DS000459.pdf
- ^{xxv} West JB. *Respiratory Physiology : The Essentials*. 9th ed. Philadelphia: Wolters Kluwer Health/Lippincott Williams & Wilkins; 2012.
- ^{xxvi} SiliconLabs. (2017, April 26). Si7021-A20 Datasheet. <https://www.silabs.com/documents/public/data-sheets/Si7021-A20.pdf>
- ^{xxvii} Dragonieri S, Schot R, Mertens BJ, Le Cessie S, Gauw SA, Spanevello A, Resta O, Willard NP, Vink TJ, Rabe KF, Bel EH, Sterk PJ. An electronic nose in the discrimination of patients with asthma and controls. *J Allergy Clin Immunol*. 2007 Oct;120(4):856-62. doi: 10.1016/j.jaci.2007.05.043.
- ^{xxviii} Paleczek, A.; Grochala, D.; Rydosz, A. Artificial Breath Classification Using XGBoost Algorithm for Diabetes Detection. *Sensors* **2021**, *21*, 4187. <https://doi.org/10.3390/s21124187>
- ^{xxix} InvenSense. (2013, September 19). MPU 6000 Datasheet. <https://invensense.tdk.com/wp-content/uploads/2015/02/MPU-6000-Datasheet1.pdf>
- ^{xxx} Massaroni, C., Nicolò, A., Lo Presti, D., Sacchetti, M., Silvestri, S., & Schena, E. (2019). Contact-based methods for measuring respiratory rate. *Sensors*, 19(4), 908. <https://doi.org/10.3390/s19040908>
- ^{xxxi} Kaplan S, Meyer D, Miranda-Dominguez O, Perrone A, Earl E, Alexopoulos D, Barch DM, Day TKM, Dust J, Eggebrecht AT, Feczkó E, Kardan O, Kenley JK, Rogers CE, Wheelock MD, Yacoub E, Rosenberg M, Elison JT, Fair DA, Smyser CD. Filtering respiratory motion artifact from resting state fMRI data in infant and toddler populations. *Neuroimage*. 2022 Feb 15;247:118838. doi: 10.1016/j.neuroimage.2021.118838.
- ^{xxxi} Khan, A. M., Lee, Y. K., Lee, S. Y., & Kim, T. S. (2010). A triaxial accelerometer-based physical-activity recognition via augmented-signal features and a hierarchical recognizer. *IEEE Transactions on Information Technology in Biomedicine*, 14(5), 1166-1172. <https://doi.org/10.1109/TITB.2010.2051955>
- ^{xxxi} Yahoo Finance. (n.d.). Financial Times Stock Exchange. (FTSE) stock price, news, quote & history. Retrieved May 2, 2023, from <https://finance.yahoo.com/quote/FTSE>
- ^{xxxiv} Sihotang, H. T., Efendi, S., Zamzami, E. M., & Mawengkang, H. (2020). Design and Implementation of Rivest Shamir Adleman's (RSA) Cryptography Algorithm in Text File Data Security. *Journal of Physics: Conference Series*, 1641. <https://doi.org/10.1088/1742-6596/1641/1/012042>
- ^{xxv} P. Gauravaram, "Security Analysis of salt||password Hashes," *2012 International Conference on Advanced Computer Science Applications and Technologies (ACSAT)*, Kuala Lumpur, Malaysia, 2012, pp. 25-30, doi: 10.1109/ACSAT.2012.49.
- ^{xxvi} Gottlieb, Irving Gottlieb (1997). *Practical Oscillator Handbook*. US: Elsevier. p. 151. ISBN 0750631023.
- ^{xxvii} Grover, Frederick W. *Inductance calculations: working formulas and tables*. Courier Corporation, 2004.
- ^{xxviii} Strang, Gilbert. "Wavelets." *American Scientist*, vol. 82, no. 3, 1994, pp. 250–55. *JSTOR*, <http://www.jstor.org/stable/29775194>. Accessed 13 June 2023.
- ^{xxix} "PicoScope Oscilloscopes: Streaming Mode." Pico Technology, 2023, <https://www.picotech.com/library/oscilloscopes/streaming-mode>. Accessed 29 May 2023.
- ^{xl} "PCNT (Pulse Counter) - ESP32 - — ESP-IDF Programming Guide latest documentation." Espressif Systems, 2023, <https://docs.espressif.com/projects/esp-idf/en/latest/esp32/api-reference/peripherals/pcnt.html>.
- ^{xli} Lin CY, Wang YW, Setiawan F, Trang NTH, Lin CW. Sleep Apnea Classification Algorithm Development Using a Machine-Learning Framework and Bag-of-Features Derived from

- Electrocardiogram Spectrograms. J Clin Med. 2021 Dec 30;11(1):192. doi: 10.3390/jcm11010192. PMID: 35011934
- ^{xlii} Neff RA, Wang J, Baxi S, Evans C, Mendelowitz D. Respiratory sinus arrhythmia: endogenous activation of nicotinic receptors mediates respiratory modulation of brainstem cardioinhibitory parasympathetic neurons. Circ Res. 2003 Sep 19;93(6):565-72. doi: 10.1161/01.RES.0000090361.45027.5B. Epub 2003 Aug 7. PMID: 12907666.
- ^{xliii} Heart Rate and Breathing Are Not Always in Phase During Resonance Frequency Breathing - Scientific Figure on ResearchGate. Available from: https://www.researchgate.net/figure/Examples-of-phase-relationships-between-heart-rate-and-breathing-for-particular_fig2_340612756
- ^{xliv} Anders Hast; Johan Nysjö; Andrea Marchetti (2013). Optimal RANSAC – Towards a Repeatable Algorithm for Finding the Optimal Set. Available from: <http://www.cb.uu.se/~aht/articles/A53-full.pdf>
- ^{xlv} Tripepi G, Jager KJ, Stel VS, Dekker FW, Zoccali C. How to deal with continuous and dichotomic outcomes in epidemiological research: linear and logistic regression analyses. Nephron Clin Pract. 2011;118(4):c399-406. doi: 10.1159/000324049. Epub 2011 Feb 23. PMID: 21346375.
- ^{xvi} Yu, Hao, and Bogdan M. Wilamowski. "Levenberg–marquardt training." *Intelligent systems*. CRC Press, 2018. 12-1.
- ^{xvii} How2Electronics. (n.d.). Power Supply for ESP32 with Boost Converter & Battery Charger. Retrieved May 5, 2023, from <https://how2electronics.com/power-supply-for-esp32-with-boost-converter-battery-charger/>
- ^{xviii} Federal Communications Commission. (n.d.). Radio Frequency Safety. <https://www.fcc.gov/general/radio-frequency-safety-0>
- ^{xlix} General Data Protection Regulation (GDPR). (2022, September 27). Official Legal Text. <https://gdpr-info.eu/>